Available online at www.sciencedirect.com
SCIENCE DIRECT
ELSEVIER
Icarus 183 (2006) 135–152
ICARUS
www.elsevier.com/locate/icarus

Saturn lightning recorded by Cassini/RPWS in 2004

G. Fischer [a,*], M.D. Desch [b], P. Zarka [c], M.L. Kaiser [b], D.A. Gurnett [d], W.S. Kurth [d], W. Macher [a], H.O. Rucker [a], A. Lecacheux [c], W.M. Farrell [b], B. Cecconi [d]

[a] *Space Research Institute, Austrian Academy of Sciences, Schmiedlstr. 6, A-8042 Graz, Austria*
[b] *NASA Goddard Space Flight Center, 8800 Greenbelt Road, Greenbelt, MD 20771, USA*
[c] *Observatoire de Paris–Meudon, 5 Place Jules Janssen, 92195 Meudon Cedex, France*
[d] *Department of Physics and Astronomy, University of Iowa, 203 Van Allen Hall, Iowa City, IA 52242, USA*

Received 19 October 2005; revised 13 February 2006

Available online 11 April 2006

Abstract

During 2004 the Cassini/RPWS (Radio and Plasma Wave Science) instrument recorded about 5400 SEDs (Saturn Electrostatic Discharges), which were organized in 4 storm systems and 95 episodes. A computer algorithm with different intensity thresholds was applied to extract the SEDs from the RPWS data, and a statistical analysis on the main characteristics of these SEDs is performed. Compared to the SEDs recorded by the Voyagers in the early 1980s, some characteristics like SED rate, intensity, signal duration, or power spectrum are similar, but there are also remarkable differences with regard to time occurrence and frequency range: The first appearance of SEDs (storm 0) was recorded by RPWS from a distance of more than 300 Saturn radii at the end of May 2004, followed by storm A in mid-July, storm B at the beginning of August, and the most prominent storm C throughout most of September. There were also significant intervals of time with no detectable SED activity, e.g., SEDs were practically absent from October 2004 until June 2005. No clear indication for SEDs below a frequency of 1.3 MHz could be found. We suggest that the SED storms A, B, C, and possibly also storm 0 originate from the same storm system residing at a latitude of 35° South, which lasted for several months, waxed and waned in strength, and rotated with the Voyager radio period of Saturn. The SED source might be located in the updrafting water clouds beneath the visible cloud features detected in the Cassini images.

Keywords: Saturn; Saturn, atmosphere

1. Introduction

Impulsive radio discharges near Saturn were first detected by the Voyager 1 PRA (Planetary Radio Astronomy) experiment during the Voyager 1 Saturn encounter in November 1980 (Warwick et al., 1981; Evans et al., 1981). After ruling out any sort of spacecraft interference Warwick et al. (1981) concluded that the bursts are short-duration with a very large bandwidth, but in the time–frequency spectrum they appear narrow-banded due to the fact that they are detected only in the few channels being sampled during the short duration of the burst. The bursts were named SEDs (Saturn Electrostatic Discharges), and for Voyager 1 they extended in frequency from 20 kHz up to the upper frequency limit of the PRA receiver of 40 MHz.

For the Voyager 1 flyby the SEDs were organized in episodes with a recurrence period of 10 h and 10 min. Several months later SED episodes were also detected by Voyager 2 with a shorter period of 10 h. Both periods are remarkably shorter than the rotation rate of Saturn with 10 h 39.2 min inferred from the periodicity of Saturn Kilometric Radiation (SKR) (Desch and Kaiser, 1981). The Voyager 2 photopolarimeter detection of a narrow feature in Saturn's B ring combined with the appropriate Keplerian revolution period of about 10 h led Evans et al. (1982) to conclude that this ring feature might be responsible for the SED bursts. Later some authors favored lightning in atmospheric storms against the exotic ring mechanism to be the source of SEDs (Burns et al., 1983; Evans et al., 1983), as the saturnian atmosphere at the equator showed prograde wind speeds up to 450 m s^{-1} corresponding

* Corresponding author.
E-mail addresses: gf@space.physics.uiowa.edu, georg.fischer@oeaw.ac.at (G. Fischer).

0019-1035/$ – see front matter
doi:10.1016/j.icarus.2006.02.010

also to a period of 10 h 10 min. Finally, Kaiser et al. (1983) showed mainly with an argument of visibility that the characteristics of SEDs are best explained by a long-lived atmospheric equatorial lightning storm system with a longitudinal extension of about 60°. SEDs appeared organized in episodes lasting for about 7 h at consecutive Saturn rotations, and there was an "occultation" time typically greater than 3 h during which the storm was on the other side of the planet.

From the lower limit of the SED frequency range, which was generally around 1 MHz on the nightside and a few MHz on the dayside, Kaiser et al. (1983) and Zarka (1985a) inferred ionospheric electron densities for Saturn. Recently Mendillo et al. (2005) used a new Saturn Thermosphere–Ionosphere Model to simulate the electron densities in Saturn's ionosphere, and they found radio frequency windows produced by ring shadowing, but until now no self-consistent model has been found to match the SED observations. The anomalous low-frequency events down to 20 kHz, which were only obtained at the southernmost extremity of Voyager 1st closest approach, were explained by a reduction of the ionospheric electron density at latitudes between −23° and −39° South. At these latitudes a reduction of the ionospheric electron density to 1 or 2% of the equatorial density at the same local time would be required, which could be caused by the fact that the ionosphere at these latitudes is magnetically connected to Saturn's rings which could act as an effective sink for ionospheric plasma (Kaiser et al., 1983). We note that the low-frequency limit for the SEDs detected by Cassini/RPWS in 2004 is 1.3 MHz, and Cassini will reach higher latitudes exceeding 23° in late 2006.

Zarka and Pedersen (1983) made a statistical study of the SEDs and reported the detection of 18,000 events by Voyager 1 and 5000 events by Voyager 2, the latter being reduced by 5 to 10 dB in intensity compared to the former. They also determined the duration of events, being about 30 ms (PRA integration time for one measurement at a certain frequency channel) to 450 ms with an average value of 55 ms. The average spectral power emitted during one event was about 100 W Hz^{-1} for the Voyager 1 and 10 W Hz^{-1} for the Voyager 2 encounter. The signal intensities from the SEDs were quite strong with maximum intensities around closest approach up to 30 dB above background, and there was a clear fall-off of intensities with distance from Saturn. Zarka and Pedersen (1983) also calculated a true spectrum for the SEDs, where it turned out that the spectral power is practically constant with frequency from 5 to 26 MHz.

Optical lightning flashes have been repeatedly verified on Jupiter, and radio emissions associated with lightning have been detected on Saturn and Uranus and possibly on Venus and Neptune as well (Desch et al., 2002). In the case of Jupiter, optical lightning signals were first detected by Voyager 1 (Cook et al., 1979), and whistler signals were also detected throughout both Voyager Jupiter encounters (Gurnett et al., 1979). On the other hand no HF (high frequency) radio signals were detected at Jupiter, which Zarka (1985b) explains by strong absorption suffered by the radio waves propagating through Jupiter's lower ionospheric layers. For Saturn the SEDs represent the HF radio part, whereas no whistlers were detected by the Voyagers. For the SEDs detected in 2004 and presented in this work, Cassini was far outside the magnetosphere. Hence, whistlers associated with these SEDs cannot be expected, as whistlers propagate along the magnetic field lines of a planet.

2. The instrument and its modes

The RPWS (Radio and Plasma Wave Science) instrument onboard Cassini is a considerably more complex instrument than the Voyager PRA. It consists of three electric monopole antennas E_u, E_v, E_w of 10 m in length, three magnetic antennas, a Langmuir probe, plus a system of receivers for various frequency ranges. Additionally, the monopoles E_u and E_v can be combined to form the dipole E_x (Gurnett et al., 2004; Cecconi and Zarka, 2005). For SED detection the most important receiver is the High Frequency Receiver (HFR), and here especially the HF1 and HF2 bands, which act as sweeping receivers: HF1 can sweep through a frequency range of 125–4125 kHz in $n \times 25$ kHz steps, and HF2 goes from 125 to 16,125 kHz in $n \times 50$ kHz steps, with n being a positive integer. For both HF1 and HF2 the bandwidth is 25 kHz, and it is possible to have 1, 2, 4, or 8 linearly spaced channels within this bandwidth. Selectable integration times are 20, 40, 80, or 160 ms for HF1, and 10, 20, 40, or 80 ms for HF2 (Gurnett et al., 2004).

Despite the various possibilities there were just a few mode settings, which were used in 2004 for the HF1 and HF2 bands. For HF1 a start frequency of 325 kHz and stop frequencies of 1800, 2025, or 4075 kHz were chosen for most of the measurement time, and auto- and cross-correlation measurements between the E_x dipole and the E_w monopole antennas was the preferred antenna mode, which allows a polarization measurement of the emissions. Another mode was the 3-antenna direction-finding (DF) mode, where one receiver toggles rapidly between the monopoles E_u and E_v and the second is connected to E_w. In this way auto- and cross-correlation measurements between E_u and E_w and shortly afterwards between E_v and E_w are performed, allowing a direction-finding without any prior assumption about the wave polarization (Vogl et al., 2004). As the low-frequency limit for the SEDs recorded in 2004 was 1.3 MHz, the SEDs were detected in the HF1 band in fact only during most of the episodes of storms A and B (see Table 1), where the high-frequency limit of HF1 was at 4025 kHz. Here the instrument was in the 3-antenna DF mode with frequency steps of 50 kHz and an integration time of 80 ms in HF1. With this long integration time nearly all bursts in HF1 were one-pixel events, which means that they were just recorded in a single frequency channel at a certain time. For shorter integration times the HF1 band was generally much noisier than HF2.

95% of all SED events in 2004 were detected within the HF2 band of the HFR, where the start frequency was mostly 1825, 2075, or 4025 kHz (adjacent to the HF1 stop frequency). The receiver made a scan through the HF2 band to the upper frequency limit of 16,025 kHz with the preferred frequency step sizes of 100 kHz ($n = 2$) or 200 kHz ($n = 4$). The time for a scan through the whole HF2 frequency range can vary significantly depending on the start frequency, the frequency step size, and the integration time. A pause of several seconds is

Table 1
Characteristics of the episodes of storms 0, A, B, and IE (irregular or isolated episodes, see text) of 2004

Episode name	DOY center	Hour center [hh:mm]	Duration from–to [hh:mm]	Time gap episodes [Sat. rot.]	Number of SEDs	True rate [h^{-1}]	Mean intensity [dB]	Mean distance [R_S]	Western long. [°] center
IE1	140	05:45	04:38–06:41	0.00	6	33	2.09	377.640	291.9
01	147	05:58	05:28–06:56	15.79	3	23	1.44	321.749	214.5
02	147	16:43	16:03–17:19	1.01	4	35	1.63	318.157	217.9
03	148	03:07	02:04–04:27	0.98	13	60	1.73	314.680	209.2
04	148	12:58	11:53–14:35	0.92	26	107	1.67	311.385	182.1
05	149	11:20	10:42–11:49	2.10	7	69	2.00	303.917	217.5
06	150	19:28	18:26–19:53	3.01	14	108	1.59	293.189	222.8
07	151	04:51	03:32–06:29	0.88	40	150	1.88	290.046	180.2
08	152	23:28	23:06–23:53	4.00	4	57	1.91	275.763	179.8
IE2	167	05:26	03:59–07:07	32.09	10	36	2.05	158.543	211.3
IE3	167	15:10	15:00–15:23	0.91	4	114	3.27	155.105	180.0
IE4	176	14:11	13:21–15:02	20.18	3	39	2.91	75.828	241.8
A1	195	04:16	02:28–07:13	41.86	414	322	2.31	79.850	225.0
A2	195	14:31	13:13–17:00	0.96	134	131	2.36	81.461	211.5
A3	196	01:18	23:50–03:15	1.01	39	42	2.28	83.116	215.4
A4	196	11:38	10:55–12:32	0.97	10	23	2.09	84.668	204.1
A5	197	08:50	08:03–09:51	1.99	29	60	2.29	87.758	200.3
A6	197	19:12	18:52–19:37	0.97	3	15	1.98	89.222	190.1
A7	199	15:59	15:18–16:35	4.20	6	17	2.30	95.226	262.1
A8	200	02:14	00:40–03:41	0.96	55	68	3.48	96.533	248.4
A9	200	12:37	11:23–14:06	0.97	32	44	2.45	97.830	238.8
A10	200	22:38	21:13–00:41	0.94	12	13	3.79	99.069	217.3
A11	201	09:48	08:33–11:25	1.05	21	27	2.53	100.455	234.5
A12	202	07:07	06:24–08:00	2.00	7	16	2.99	102.952	234.1
A13	203	05:03	03:45–06:55	2.06	8	9	2.04	105.425	254.7
A14	204	02:46	02:37–03:05	2.04	4	31	2.04	107.784	268.5
A15	209	20:55	20:02–22:16	12.96	7	12	1.91	120.866	253.9
B1	216	01:09	00:09–02:30	13.91	9	14	1.81	131.748	220.0
B2	216	11:39	10:37–13:37	0.99	13	16	1.92	132.410	214.9
B3	216	23:04	21:45–00:20	1.07	20	29	2.10	133.113	240.3
B4	217	08:20	07:06–09:15	0.87	16	28	1.58	133.673	193.5
B5	217	19:13	18:50–19:52	1.02	10	36	2.37	134.317	201.2
B6	218	17:44	16:44–18:54	2.11	9	15	1.49	135.603	241.5
B7	219	04:42	03:25–05:37	1.03	42	71	2.27	136.208	251.8
B8	219	13:57	13:00–15:09	0.87	24	41	2.12	136.707	204.2
B9	220	01:26	23:53–02:39	1.08	17	23	2.04	137.313	232.3
B10	220	12:38	11:59–13:28	1.05	4	10	1.94	137.889	250.4
IE5	220	18:42	17:02–20:07	0.57	13	16	2.83	138.195	95.3
IE6	221	05:21	04:55–05:37	1.00	3	16	3.30	138.723	95.0
B11	221	09:58	08:26–10:36	0.43	6	10	2.21	138.947	251.0
B12	226	16:33	15:57–17:26	11.88	11	28	2.06	144.195	206.5
B13	227	04:02	02:42–04:57	1.08	23	38	2.03	144.586	234.1
B14	227	14:40	13:34–15:51	1.00	24	39	2.39	144.936	233.4
B15	228	00:48	00:06–01:31	0.95	23	60	2.69	145.259	215.9
B16	228	11:27	10:34–12:41	1.00	18	32	2.39	145.587	215.4

Note. In successive columns we list the name of the episode, the day of year (DOY), the hour of the center time of an episode (mean time of SEDs belonging to this episode), the start and stop time of the episode, the time gap between the center times of the previous and the current episode expressed in Saturn rotations, the number of SEDs of the respective episode, the true SED burst rate in number of SEDs per hour, the mean intensity of these SEDs in dB above the background, the mean distance to the surface of Saturn in Saturn radii [R_S], and the sub-spacecraft western longitude at the center time of the episode.

normally made after one scan, and a new scan was started very often every 16 or 32 s. All four possible integration times were used, the shortest one with 10 ms was sporadically applied in the months before SOI (Saturn Orbit Insertion), but only one irregular SED episode (IE4 on DOY 176, see Table 1) consisting of just 3 bursts was detected in this mode.

Storm 0 at the end of May was recorded with an integration time of 20 ms in the dipole mode E_x (no polarization or direction of the incoming wave can be retrieved), an HF2 start frequency of 1825 kHz, and a frequency step size of 200 kHz. Fig. 1 shows the SEDs of episode 07 of this storm, where due to the short integration time the bursts have several pixels in length. The episodes from both storms A and B were recorded in the 3-antenna DF mode using an HF2 start frequency of 4025 kHz, a frequency step size of 200 kHz, and an integration time of 80 ms. Due to the long integration time only very few bursts consisted of two or more pixels. Finally, all the episodes of the most prominent storm C in September

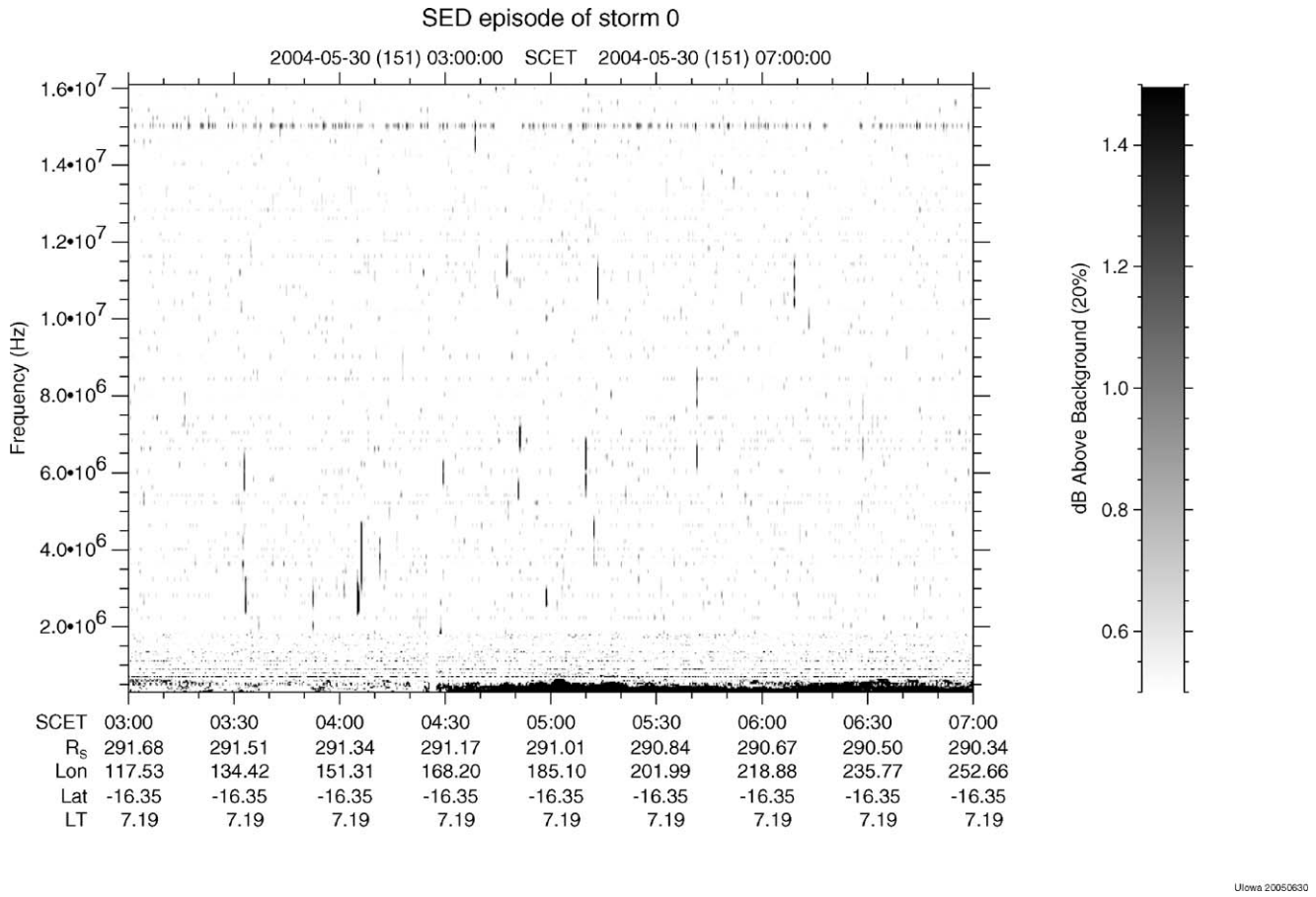

Fig. 1. Dynamic spectrum over 4 h recorded by Cassini/RPWS showing the episode 07 of storm 0. Spacecraft event time (SCET), distance in Saturn radii, sub-spacecraft western longitude and latitude, and local time of the spacecraft are given along the time axis.

2004 were recorded using the dipole mode E_x with a start frequency of 1825 kHz, a frequency step size of 100 kHz, and an integration time of 40 ms. 3-Antenna DF during this September storm was only shortly applied around DOY 264 but not during an SED episode.

When calculating the SED occurrence rates we have to take into account the instrument mode, because the SED frequency range is only covered for a limited time. Therefore, we estimate the duty cycle of the instrument for frequencies above 1.8 MHz: For storm 0 with an integration time of 20 ms there were 72 frequency steps at HF2, and there was one scan every 16 s, which gives a duty cycle of $(72 \times 0.020)/16 \approx 0.09$. Similarly for the integration time of 40 ms used for storm C we had 143 frequency steps at HF2 every 16 seconds leading to $(143 \times 0.040)/16 \approx 0.36$. It is a little bit more complicated for storms A and B for the DF-mode with 80-ms integration time: We had 45 frequency steps in HF1 from 1.8 to 4.0 MHz plus 61 steps at HF2, and this only every 32 s, hence $(45 + 61) \times 0.080/32 \approx 0.27$.

3. Data analysis method

3.1. Intensity thresholds as a function of HFR integration time

Due to the large quantity of data, a computer algorithm was applied to extract the SEDs: The measured spectral intensity $S_{i,j}$ (given in $\mathrm{V^2\,Hz^{-1}}$) can be stored in an $(i \times j)$-matrix, where the rows i correspond to different frequencies, and the columns j correspond to successive frequency scans at different times. As already mentioned, a short-duration burst results in a vertical streak in the time–frequency spectrum. Such a short signal can be recorded in several frequency channels, but only during one frequency scan as the time between the scans is in general much longer than the signal duration.

Zarka and Pedersen (1983) compared each data point in a given frequency channel to the average of the previous and the following data point in the same channel with the same polarization state. As the PRA receiver alternatively measured left- and right-handed circular polarization every 6 s, each data point $S_{i,j}$ was compared to the average of the scans 12 s before (2 scans before: $S_{i,j-2}$) and after (2 scans afterwards: $S_{i,j+2}$). If $S_{i,j}$ was a certain threshold (1 dB corresponding to a factor of 1.26) above the mean $(1/2)(S_{i,j-2} + S_{i,j+2})$, the pixel $S_{i,j}$ was considered as an SED event. It is obvious that the threshold at which a signal is regarded as an SED event is a very important parameter which has to be set in accordance with the fluctuation of the background. If the threshold is set too high, several low-intensity bursts will not be counted as SEDs. On the other hand, if the threshold is set too low, several low-intensity events, which are just caused by the natural fluctuation of the background, will be regarded as SEDs and misrepresent our sta-

tistical investigation. The fluctuation σ (standard deviation) of the background depends on the following physical parameters:

$$\sigma = \frac{2k_{\mathrm{B}}T}{A_{\mathrm{eff}}\sqrt{\Delta f\,\Delta t}} \tag{1}$$

with k_{B} as Boltzmann's constant, T as the antenna temperature, A_{eff} as the antenna effective area, Δf as the receiver bandwidth, and Δt as the integration time. For the HF1 and HF2 band of the RPWS/HFR, $\Delta f = 25$ kHz has a constant value, but as listed in the previous section different integration times Δt can be chosen. It is clear from the equation above that a longer integration time results in less background fluctuation. We assume that the background radiation has a Gaussian distribution (as a consequence of the central limit theorem) with a median value $\bar{B}$ and a standard deviation σ. Fig. 3c in Zarka et al. (2004) shows a histogram of intensities, where it can be seen that the galactic background noise can be well approximated by a Gaussian distribution. We demand a signal intensity greater than 4σ above the median background value $\bar{B}$ for a signal to be regarded as an SED. For Cassini/RPWS there is no alternative measurement of left- and right-handed polarization, hence we compare the intensities of $S_{i,j-1}$ and $S_{i,j+1}$ with the intensity at $S_{i,j}$, and we applied the following three criteria (logical AND):

$$S_{i,j} > f_{4\sigma}\,S_{i,j-1} \quad \text{AND} \quad S_{i,j} > f_{4\sigma}\,S_{i,j+1} \quad \text{AND} \quad S_{i,j} > f_{4\sigma}\,\bar{B} \tag{2}$$

with $f_{4\sigma}$ as a threshold factor that has to be calculated from the standard deviation σ of the background and that also depends on the receiver integration time. With these three conditions (2) we use a more strict criterion than Zarka and Pedersen (1983): We not only demand that the SED pixel $S_{i,j}$ has to be 4σ above the background $\bar{B}$, but also both the intensity $S_{i,j-1}$ at the previous frequency scan AND the intensity $S_{i,j+1}$ at the next scan have to be at least 4σ below the intensity of the SED pixel. An illustration of the comparison of signal intensity levels at a fixed frequency channel at successive scans can be seen in Fig. 2. We note that the peak signal on the left side of Fig. 2 would be recognized as an SED event, whereas the signal (i, j) at the right side would be rejected by our algorithm as the signal intensity at $(i, j+1)$ is not 4σ below the signal level at (i, j), but the algorithm of Zarka and Pedersen (1983) would accept it as an SED event.

The usage of the 4σ-threshold can be justified in the following way: In the symmetric Gaussian distribution about

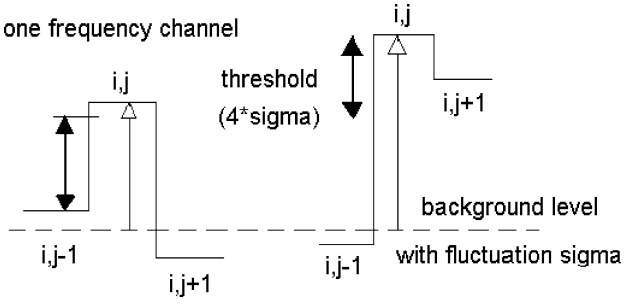

Fig. 2. Illustration of signal intensity levels at a fixed frequency channel during successive scans.

99.9968% of all values lie below the median value plus 4 standard deviations ($\bar{B} + 4\sigma$), and only 0.0032% of all values should exceed $\bar{B} + 4\sigma$. Additionally we assume that the two neighboring pixels are also at least 4σ below the SED pixel, so on average each of them should lie below the median background value $\bar{B}$, and the probability for this is $\frac{1}{2} \times \frac{1}{2} = \frac{1}{4}$ as half the values lie below $\bar{B}$. So without any SED activity or other signals it can be expected that only $0.0032\%/4 = 0.0008\%$ of all measurement values fulfill the three conditions of Eq. (2) just due to the natural fluctuation of the background. Typically (for example for the instrument mode applied at the storm C), we have one scan every 16 s (5400 scans per day) at 143 frequency channels resulting in $5400 \times 143 = 772{,}200$ measurements (pixels) per day, and hence only $772{,}200 \times 0.000008 = 6$ pixels per day fulfilling the criteria of Eq. (2) can be expected to be due to the natural fluctuation of the background. These 6 events can happen at any time, and such single events of low intensity, which did not take place during an SED episode, were mostly removed manually from the list of SEDs. From a similar consideration it becomes evident that a threshold of only 3σ would be not enough, because this would lead to a number of 260 false events per day. We tested our computer algorithm also with a 3σ-threshold, and as expected several events were recognized at any time especially between SED episodes, where no events had been identified with the 4σ-threshold.

Fig. 3 shows the value of the 4σ-threshold level in dB above the median background as a function of time. The standard deviation σ and the "median" background level $\bar{B}$ were calculated hourly at each frequency channel. All intensity values of 1 h of measurement were converted into a decibel scale, and $\bar{B}$ was calculated as the mean intensity of all signals after the elimination of stronger and weaker signals lying outside of $\pm 4\sigma$ around the most frequent intensity. The standard deviations were calculated for each frequency channel. Then their values, given in dB, were multiplied by 4 and a mean value of this 4σ-threshold was calculated over all frequencies above 1.8 MHz. This is the quantity that is plotted at the y-axis of Fig. 3. It can be clearly seen that this 4σ-threshold level behaves in a step-like fashion, where the steps occur at exactly those times, where the integration time of the receiver was changed. The various peaks and fluctuations in Fig. 3 are due to different integration times for short time intervals, intense solar bursts, or other interferences raising the calculated standard deviations. In case of no data the standard deviation in Fig. 3 was set to zero.

From Eq. (1) we can get a theoretically predicted ratio of the fluctuation for two different integration times, assuming that all other parameters except Δt are constant:

$$\frac{\sigma_{20\ \mathrm{ms}}}{\sigma_{10\ \mathrm{ms}}} = \frac{\sigma_{40\ \mathrm{ms}}}{\sigma_{20\ \mathrm{ms}}} = \frac{1}{\sqrt{2}} \approx 0.71. \tag{3}$$

From Fig. 3 we get the following values of the 4σ-threshold: around 1.34 dB for 10 ms, 1.00 dB for 20 ms, 0.75 dB for 40 ms, and interestingly the high value of 1.12 dB for the longest integration time of 80 ms. Using these values we calculate the

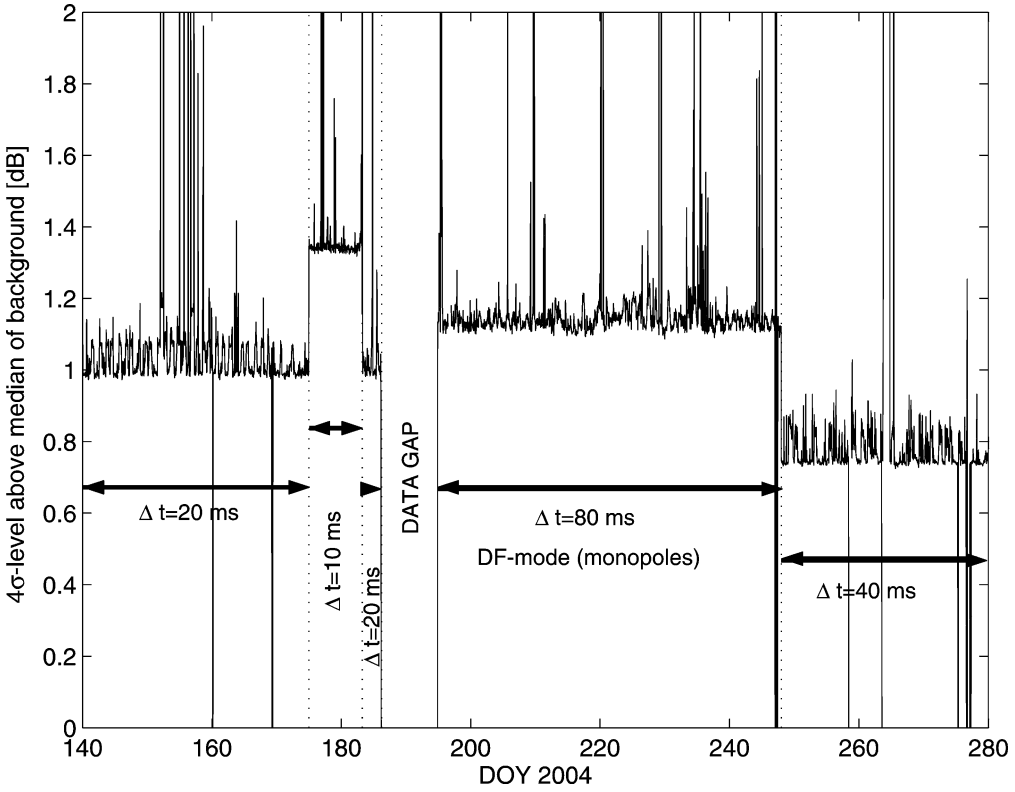

Fig. 3. Hourly calculated 4σ-background fluctuation level in dB above the median background as a function of the DOY (day of year) 2004.

fluctuation ratios for the different integration times after some algebra with the following equations:

$$\frac{\sigma_{20\text{ ms}}}{\sigma_{10\text{ ms}}} = \frac{10^{\frac{1.00}{4\times 10}} - 1}{10^{\frac{1.34}{4\times 10}} - 1} \approx 0.74 \quad \text{and}$$

$$\frac{\sigma_{40\text{ ms}}}{\sigma_{20\text{ ms}}} = \frac{10^{\frac{0.75}{4\times 10}} - 1}{10^{\frac{1.00}{4\times 10}} - 1} \approx 0.74, \tag{4}$$

which is very close to the theoretically predicted value of $\frac{1}{\sqrt{2}}$. The high fluctuation level for the integration time of $\Delta t = 80$ ms can be explained by the fact that only in the DF-mode with $\Delta t = 80$ ms the monopoles are used, whereas at all other integration times the dipole is used. The monopole has approximately half of the effective area of the dipole, hence the fluctuation σ must be greater than for the dipole according to Eq. (1). (The ratio of the effective areas of the dipole and the monopole can be calculated in this way, and we found a value of 2.24.)

Finally, we note that we used the following 4σ-threshold values for the automatic SED detection with the criteria given in Eq. (2):

- $f_{4\sigma} = 1.26$ (1 dB, 20 ms) from DOY 140 to 166 and DOY 183 to 186,
- $f_{4\sigma} = 1.35$ (1.3 dB, 10 ms) from DOY 167 to 182,
- $f_{4\sigma} = 1.29$ (1.1 dB, 80 ms DF) from DOY 194 to 247,
- $f_{4\sigma} = 1.20$ (0.8 dB, 40 ms) from DOY 248 to 272.

There is a data gap from DOY 187 to DOY 194, and no clear indication of SEDs was detected in 2004 before DOY 140 and after DOY 272.

For the noisy HF1 part of the HFR we did not calculate the thresholds separately, and the computer algorithm detected a lot of spurious events, but only a few of them were SEDs where the extension of the respective SED episode down to lower frequencies could be clearly seen in the dynamic spectrum. We checked the low-frequency extension of all SED episodes visually in the dynamic spectra, but we could not find any SEDs below 1.3 MHz.

3.2. *Jovian decametric arcs, solar bursts, and other interferences*

Although the previously described algorithm works pretty well, we have to be aware that the criteria in Eq. (2) can be also fulfilled by other kinds of radio emissions as jovian arcs, solar bursts, or other sources of interference. Hence, all dynamic spectra were also checked visually and, in case of a misinterpretation, the detected events were removed manually from the list of SEDs. Solar type III bursts are quite easy to identify in the dynamic spectrum from their appearance in the time–frequency plane, where a broadband burst can extend over several minutes with a high-frequency drift. It also happens very often that close to solar bursts, narrow-banded bursts appear which look like SEDs; also these bursts were removed manually. Sometimes certain frequency channels of the HFR show an enhanced intensity fluctuation. This was the case very often at 15,025 kHz,

at 16,025 kHz, and in the DF-mode in several frequency channels around 10,025 kHz. Such bursts were also removed from the list.

Another type of emission which can mimic the SEDs are the so-called jovian decametric arcs, which are magnetospheric radio emissions from Jupiter that appear arc-like (somewhat like parentheses) in the time–frequency spectrogram. These emissions still can be detected with Cassini now in orbit around Saturn even though Jupiter is increasingly far away. Due to the large distance of Jupiter, jovian arcs do not appear as smooth emissions, but they are quite bursty and appear like peaks of mountains (intensity) above the fog layer of the galactic background radiation. In some cases they have a clear vertex, and they are quite easy to identify visually. But, this is not always the case, and it can be difficult to distinguish between jovian emissions and SED episodes. In general, within one SED episode the SEDs should be equally distributed in frequency above the ionospheric cutoff frequency, and an episode should have a duration of at least several tens of minutes and can last for several hours. On the other hand typical jovian emissions also consist of several bursty emissions, but very often they cover only a limited frequency range and a shorter time interval. An additional hint gives the phase of Io as seen from the observer Cassini: if the Io-phase is close to 90° or 270° a jovian emission is likely. In summary, we decided to use a conservative approach and counted the events only as SEDs in the cases where we were quite sure that they were not other radio emissions. For example in November, December 2004, and January 2005 there were several cases where it was difficult to decide whether some weak and bursty emissions were of jovian origin or SEDs, and we did not count them as SEDs.

4. Occurrence of saturnian lightning in time

With the computer algorithm described in the last section we have detected about 5400 SEDs in the RPWS HFR data during 2004. For the discussion of the temporal occurrence of these events, we first want to explain the difference between the terms episode and storm: The SEDs are organized in episodes, which are clusters of events over several tens of minutes to hours. We require that an episode consists of at least 3 SEDs. The episodes recur repeatedly with Saturn's rotation, and this clustering of episodes is called an SED storm system. We note that there are also some isolated bursts between the episodes, but the vast majority of SEDs (more than 99%) recorded in 2004 was clustered in the episodes listed in Tables 1 and 2. In these two tables many characteristic physical properties of all episodes from 2004 are listed in detail. There were three storm systems after Cassini SOI, which are called storms A, B, and C, occurring in mid-July, first half of August, and throughout most of September 2004, respectively (Gurnett et al., 2005). Additionally there was also one storm system about one month before SOI at the end of May, which we call the 0 (zero) storm. A diagram showing the number of SEDs of each episode from DOY 190 until DOY 280 (containing the storms A, B, and C) can be found in Gurnett et al. (2005). Similarly in Fig. 4, we show the number of SEDs of each episode in all four storm systems in four separate panels, where the different scaling of the axes should be noted. The absolute numbers of SED bursts are a little bit higher than in Gurnett et al. (2005), which is due to our refined detection algorithm. Additionally, the difference of the center times between some successive episodes are indicated in units of Saturn rotations in Fig. 4. The so-called center times listed in column 3 of Tables 1 and 2 are calculated as the mean time of all SED events within one episode. It also can be clearly seen that within one storm system the SED episodes do not occur at every Saturn rotation, and some episodes are out of phase compared to the surrounding episodes. For example, storm C seems to be divided into 2 parts, the first one from September 4 to 19 (DOY 248 to 263), and the second one from September 20 to 28 (DOY 264 to 272), because there is a gap of 4.0 Saturn rotations between the episodes C32 and C33 (see Table 2).

In Fig. 5 one can see the inbound trajectory of Cassini and the first three orbits, and the stars mark the positions of the spacecraft at the center times of the SED episodes. SEDs were first recorded from a distance of 378 Saturn radii (lower right corner of Fig. 5), and storm 0 occurred on the inbound trajectory when Cassini was on average 300 Saturn radii away. There are two isolated weak episodes on June 15 (DOY 167), and one on June 24 (DOY 176). All other episodes of the A, B, and C storms occurred when Cassini was on the morning side of Saturn during its first long orbit. We note that the western longitude system for Saturn used in this paper is based on the IAU definition (Seidelmann et al., 2002), which uses the Voyager radio period of about 10.656 h. For example in the last column of Tables 1 and 2 one can find the sub-spacecraft western longitudes at the center times of the SED episodes. Since the SEDs are an atmospheric phenomenon and some zonal belts of Saturn's atmosphere rotate approximately with the Voyager radio period ("zero wind velocity"), the usage of this system seems appropriate despite a possible slower period of the planet and its magnetic field of about 10.763 h derived from Cassini/RPWS observations (Gurnett et al., 2005). In the following subsections we briefly describe the temporal occurrence of the episodes of all SED storms.

4.1. Storm 0

Storm 0 consists of 8 episodes (named 01 to 08) from May 26 (DOY 147) until May 31 (DOY 152). There is a small episode consisting of only 6 events on May 19 (DOY 140), which were the first SEDs recorded in 2004. We named this episode IE1 (for irregular or isolated episode, see Table 1), and it occurred 15.8 Saturn rotations before the onset of storm 0. Storm 0 comprised 111 SED bursts with a mean intensity of 1.8 dB above background. The most prominent episode 07 was registered on May 30 (DOY 151) with 40 bursts within a duration of nearly 3 h. A dynamic spectrum of this episode 07 can be seen in Fig. 1. In this spectrum, and also in the spectrum in Fig. 6 of episode C43, the dark area at the bottom below ~700 kHz is Saturn Kilometric Radiation (SKR). Both spectra show an enhanced fluctuation level in the 15,025-kHz channel caused by interference. During the course of storm 0 Cassini

Table 2
Continuation of Table 1 for the episodes of storm C

Episode name	DOY center	Hour center [hh:mm]	Duration from–to [hh:mm]	Time gap episodes [Sat. rot.]	Number of SEDs	True rate [h^{-1}]	Mean intensity [dB]	Mean distance [R_S]	Western long. [°] center
C1	248	22:41	21:30–23:18	46.10	8	12	1.47	148.059	244.7
C2	249	08:54	07:58–10:32	0.96	52	56	1.74	147.867	230.1
C3	249	20:04	18:24–21:35	1.05	29	25	1.38	147.646	247.0
C4	250	06:15	05:07–07:30	0.96	32	37	1.31	147.435	230.9
C5	250	17:18	15:35–20:18	1.04	48	28	1.33	147.196	244.1
C6	251	03:50	02:35–05:17	0.99	17	18	1.42	146.957	239.5
C7	251	13:36	13:12–14:09	0.92	10	29	1.35	146.727	209.3
C8	252	01:05	23:38–03:18	1.08	25	19	1.39	146.444	237.2
C9	252	13:16	12:11–14:22	1.14	5	6	1.16	146.132	288.4
C10	252	22:38	20:58–00:52	0.88	80	57	1.43	145.882	244.9
C11	253	09:05	07:42–11:48	0.98	30	20	1.31	145.594	237.5
C12	253	19:52	18:19–22:15	1.01	123	87	1.60	145.286	241.9
C13	254	06:38	04:49–09:35	1.01	33	19	1.33	144.967	245.5
C14	254	16:31	14:55–18:31	0.93	42	32	1.51	144.665	219.0
C15	255	04:23	02:17–06:54	1.11	203	122	1.43	144.290	259.7
C16	255	13:40	12:19–15:39	0.87	39	33	1.44	143.988	213.2
C17	256	00:49	23:01–02:42	1.05	80	60	1.79	143.614	229.6
C18	256	12:19	10:10–14:52	1.08	82	48	1.35	143.215	258.1
C19	256	22:30	20:34–01:16	0.96	315	186	1.50	142.851	242.1
C20	257	08:32	07:07–11:13	0.94	141	95	1.52	142.484	220.5
C21	257	19:35	17:57–21:57	1.04	65	45	1.54	142.067	234.0
C22	258	06:27	05:01–09:08	1.02	58	39	1.55	141.645	241.0
C23	259	03:37	02:12–05:51	1.99	34	26	1.21	140.792	235.6
IE7	259	07:56	07:28–09:08	0.41	5	8	1.63	140.612	21.5
C24	259	13:48	12:11–16:19	0.55	49	33	1.70	140.365	219.2
C25	260	01:23	23:35–04:00	1.09	93	59	1.45	139.867	250.7
C26	260	11:40	10:02–14:41	0.96	161	96	1.62	139.413	237.7
C27	260	22:21	20:35–01:10	1.00	82	50	1.50	138.931	238.4
C28	261	08:49	07:23–11:43	0.98	80	51	1.58	138.447	232.0
C29	261	20:00	18:00–22:50	1.05	251	144	1.57	137.918	249.1
C30	262	05:30	04:30–06:48	0.89	105	127	1.79	137.458	210.1
C31	262	16:00	15:10–17:11	0.99	30	41	2.00	136.939	204.5
C32	263	04:41	02:41–05:41	1.19	12	11	1.54	136.296	273.0
C33	264	23:31	22:31–00:21	4.02	9	14	2.25	134.000	279.3
C34	265	09:12	07:33–11:38	0.91	49	33	1.80	133.453	246.2
C35	265	19:51	18:25–21:40	1.00	70	60	1.46	132.840	245.8
C36	266	05:15	04:52–05:53	0.88	17	46	1.91	132.288	203.3
C37	266	17:09	15:26–19:21	1.12	34	24	1.53	131.576	244.8
C38	267	03:30	01:54–05:59	0.97	49	33	1.86	130.943	234.5
C39	267	13:45	12:37–16:20	0.96	11	8	1.75	130.304	220.6
C40	268	01:00	23:41–02:32	1.06	84	82	1.63	129.590	240.4
C41	268	11:24	10:10–12:54	0.98	55	56	1.66	128.916	231.4
C42	268	22:11	20:35–00:58	1.01	108	68	1.60	128.204	235.4
C43	269	09:11	07:21–11:20	1.03	370	257	1.81	127.464	246.7
C44	269	20:11	17:49–23:22	1.03	431	216	1.85	126.709	258.2
C45	270	06:17	04:26–09:01	0.95	322	196	1.69	126.003	239.3
C46	270	17:12	15:43–20:13	1.02	79	49	1.80	125.226	247.5
C47	271	03:32	02:43–04:49	0.97	7	9	1.34	124.477	236.6
C48	271	14:54	12:34–17:51	1.07	43	23	1.84	123.637	260.5
C49	272	12:13	10:56–13:19	2.00	15	17	1.67	122.019	260.1

was approaching Saturn from a distance of 322 to 275 Saturn radii at a practically constant local time of about 7.2 LT.

4.2. Storm A

As already mentioned, there are three weak and isolated episodes IE2, IE3, and IE4 between storm 0 and storm A. IE2 and IE3 on June 15 (DOY 167) are in fact separated by 0.9 Saturn rotations from each other, and their centers appear at sub-spacecraft western longitudes of 211° and 180°, respectively. Also IE4 on June 24 (DOY 176) appears at a similar longitude (242°), hence, all three isolated episodes are approximately in phase with the episodes of storm 0 before and storm A afterwards. No SEDs could be identified during SOI. Storm A started on July 13 with the very strong episode A1 lasting nearly for 5 h with 414 detected SEDs. There is only one more episode

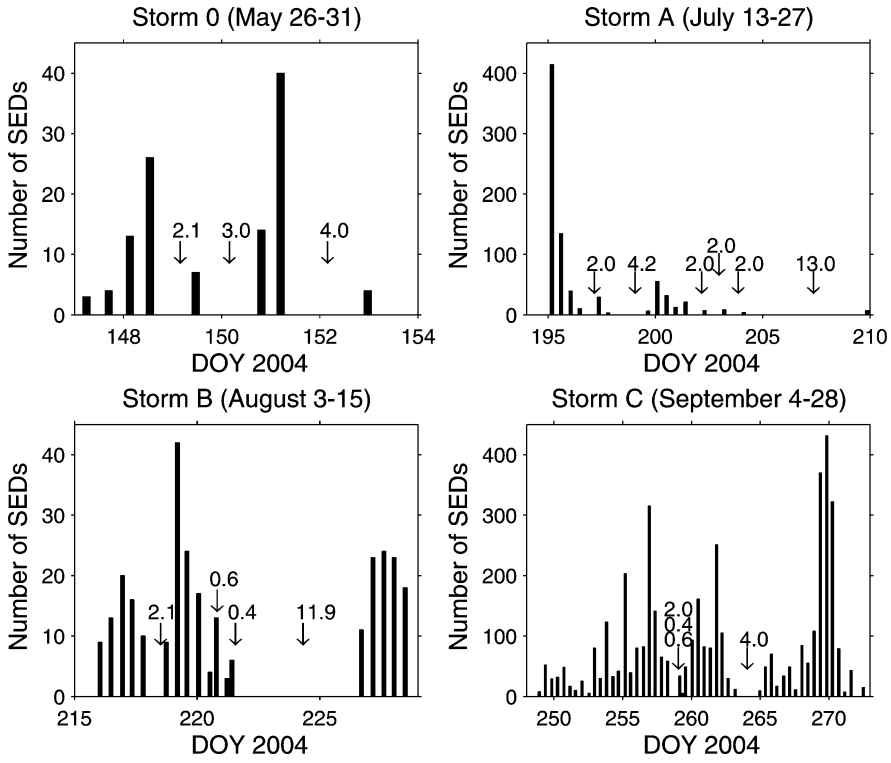

Fig. 4. Number of SEDs per episode as a function of time for the 4 storms in 2004. The numbers with the arrows in the figure represent the time differences between the center times of two successive episodes counted in Saturn rotations.

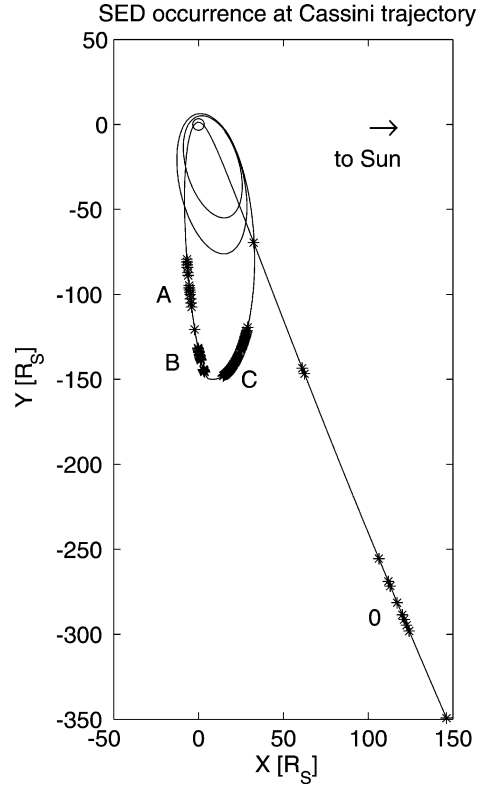

Fig. 5. Trajectory of Cassini inbound plus the first 3 orbits until Titan flyby TC on January 14, 2005, projected into the ecliptic plane of Saturn. The stars denote the positions of Cassini when SED episodes were recorded during the 4 storms 0, A, B, and C in 2004.

in 2004 with more than 400 SEDs, which is C44 on September 25 (DOY 269) with 431 detected events. It is possible that there were SEDs also before episode A1, but there is a data gap from DOY 186 to 194. Storm A consists of 15 episodes (A1 to A15) and lasts from July 13 (DOY 195) to July 27 (DOY 209). Nearly 800 SEDs were detected during storm A with a mean intensity of 2.4 dB above background. On DOY 200 around 22:49 SCET during episode A10 the RPWS recorded the SED burst with the highest signal intensity in 2004 with 8.1 dB above background. During the course of storm A Cassini was outbound on its first orbit (Orbit 0) going from a distance of 80 Saturn radii at A1 to 121 Saturn radii at A15 with a local time change from 5.1 to 5.4 LT. A15 on July 27 appears 13.0 Saturn rotations after A14 on July 22, and 13.9 Saturn rotations before B1 on August 3, the first episode of storm B. A15 consists of only 7 SEDs and is in fact between storm A and B (so we could also label it as an isolated episode), but it is important that it is in phase with the episodes of both storms A and B.

4.3. Storm B

Storm B lasts from August 3 (DOY 216) to August 15 (DOY 228) or maybe longer, but due to their weakness and scarcity, episodes cannot be clearly identified for about 10 days after August 15. Storm B consists of 16 episodes and about 270 events with a mean intensity of 2.2 dB above background. Storm B can be divided into at least two parts: There are 11 highly regular episodes B1–B11 from August 3 (DOY 216) to August 8 (DOY 221) appearing at consecutive Saturn rotations except between

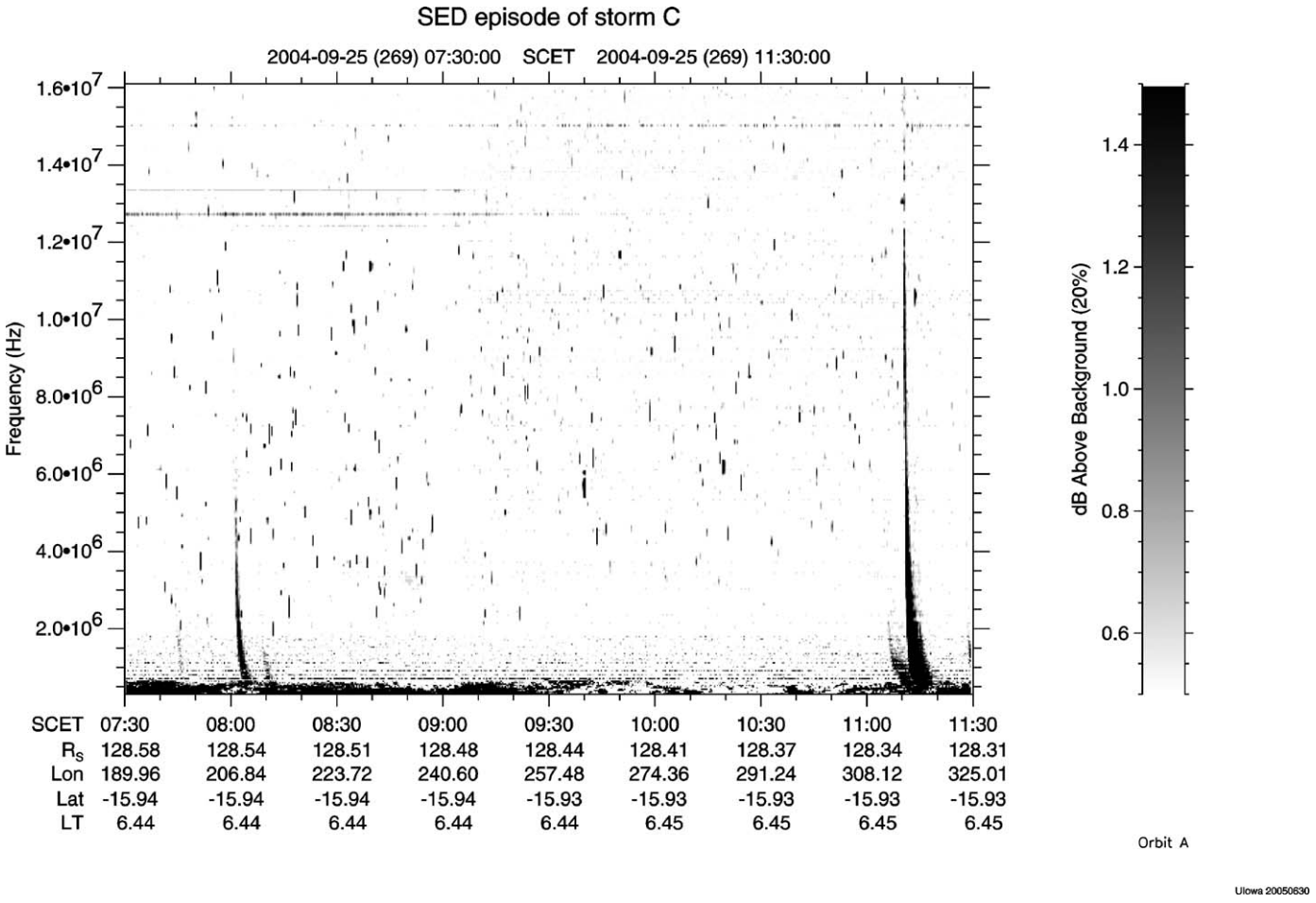

Fig. 6. Dynamic spectrum over 4 h recorded by Cassini RPWS showing the episode C43 of storm C (similar to Fig. 1).

B5–B6 and B10–B11, where in both cases the time gap is two Saturn rotations. There are two irregular episodes IE5 and IE6, which are out of phase of B1–B11, because both of their centers appear at a sub-spacecraft western longitude around 95°. Between B11 and B12 there is a gap of 11.9 Saturn rotations, and storm B finishes with 5 consecutive episodes (B12–B16) from August 13 (DOY 226) to August 15 (DOY 228). Each episode of storm B has a duration of less than 3 h and consists of just a few tens of bursts with B7 being the most prominent with 42 SEDs. During storm B the spacecraft was still outbound on its first orbit at distances of 132 Saturn radii at B1 to 146 Saturn radii at B16 with a local time change from 5.5 to only 5.6 LT.

4.4. Storm C

The most prominent storm C lasted from September 4 (DOY 248) to September 28 (DOY 272) consisting of 49 episodes. Nearly 4200 SED bursts, which is 77% of all SEDs of 2004, were recorded, and the mean SED burst intensity is 1.6 dB above the background. The episode with the greatest number of SEDs (more than 430) is episode C44 on September 25, which is surrounded by the episodes C43 and C45, each of them with more than 300 bursts. There is a third episode with more than 300 events occurring on September 12 (C19 on DOY 256). The dynamic spectrum of episode C43 can be seen in Fig. 6. Besides the vertical streaks of the SEDs there are also two solar bursts around 08:00 and 11:15 SCET in this figure. Enhanced fluctuations can be seen not only at the frequency channels of 15,025 and 12,725 kHz, but also throughout the HF1 band below 1825 kHz. There is one weak irregular out of phase episode IE7 between C23 and C24. The episodes of storm C appear during nearly all Saturn rotations, except between C22 and C23 there are 2.0 and between C32 and C33 there are 4.0 Saturn rotations. Episode C1 started a short time after Cassini apoapsis at a distance of 148 Saturn radii, and until C49 the spacecraft moved closer to 122 Saturn radii, thereby making a slight local time change from 5.9 to 6.5 LT.

4.5. Isolated or irregular episodes

Altogether there occurred 7 isolated or irregular episodes IE1 to IE7 with only 44 SEDs in total, so each episode consists of only a few bursts. These episodes appeared at times separated from the main storm systems (“isolated”) or they occurred within the storm systems but out of phase compared to the majority of the other episodes (“irregular”). IE1 is an isolated episode but also irregular as it occurred one week before the onset of storm 0 and the mean sub-spacecraft western longitude of 292° is different from the mean sub-spacecraft western longitude of storm 0 of about 194°. IE2 and IE3 are only iso-

lated but regular, IE4 is isolated but also slightly irregular, IE5 and IE6 within storm B and IE7 within storm C are only irregular. Besides these 44 bursts of IE1 to IE7 there are only 31 isolated radio bursts, which do not form an episode and do not fall into the times of the episodes listed in column 4 of Tables 1 and 2. It is possible that there exist other isolated bursts, because especially the low intensity bursts outside the episodes were removed manually from the list of SEDs as they might be just due to the natural fluctuation of the background and only isolated events of higher intensity were kept. This is the reason why the mean intensity of the 75 isolated or irregular SEDs (less than 1.4% of all SEDs from 2004) is 2.5 dB above the background, which is higher than the mean intensities of the SEDs of the four storm systems. Nevertheless it can be stated that only a few percent of SEDs lie outside the episodes from the four main storm systems 0, A, B, and C.

4.6. Storm D

As already stated in the abstract no SEDs were found after the big September 2004 storm until June 2005. Finally on June 9, 2005, the SEDs returned with a long and intense episode of about 120 radio bursts. Storm D lasted only for about one week with just 4 clear episodes D1–D4. Cassini was as close as 9 Saturn radii at the start of D1 and at 38 Saturn radii at the end of D4, and the local time of the spacecraft changed from 3.4 to 7.0 LT. As the spacecraft was much closer during storm D compared to the episodes of 2004, we got the highest signal intensities for storm D, up to 14 dB above the galactic background and a mean intensity of 5.0 dB. The events and episodes of storm D (June 2005) will be not included in any further statistics here as this paper treats all SEDs of 2004. Only in the next subsection we will further discuss the special temporal occurrence of the storm D episodes.

4.7. Duration of SED episodes and discussion

Fig. 7 contains a stacked bar plot showing the durations of all 95 SED episodes in 2004 in bins of half an hour, where the grey-scaling denotes the various storms. The episode duration is taken from Tables 1 and 2. Fig. 7 shows one of the major differences between SED episodes in the Voyager and in the Cassini era: For the Voyagers the SEDs were always present when the equatorial storm system was on the side of Saturn facing the spacecraft, and there were no or only a few SEDs for about 3–4 h when the storm (with an estimated longitudinal extent of 60°) was on the other side of the planet, hence the episodes had durations of 6–7 h. The SED episodes measured by Cassini/RPWS have a mean duration of 2 h and 53 min and there are only two episodes (C44 and C48) with a duration exceeding 5 h. Hence, unlike Voyager, it is likely that the SED sources of 2004 were localized sources with no significant longitudinal extension.

The mean intensity of all SEDs within one respective episode can be found in the 8th column of Tables 1 and 2. The mean intensity of all SEDs measured by Cassini/RPWS in 2004 is only 1.8 dB above the galactic background. For such

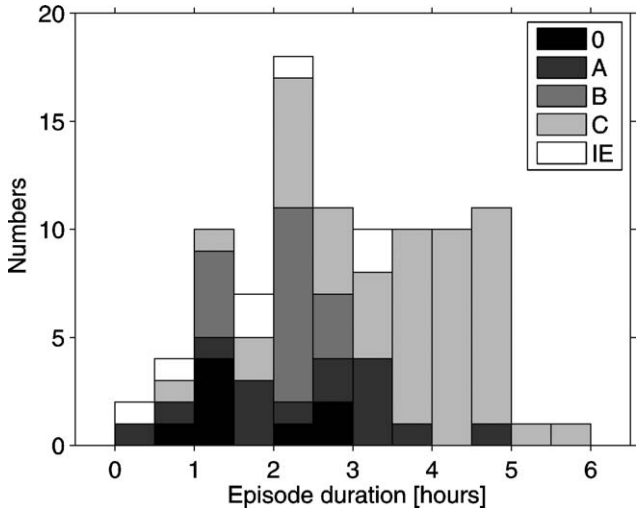

Fig. 7. Stacked bar-plot showing the duration of all SED episodes from 2004 in bins of half an hour. The grey-scale from white to black denotes storm 0 (black), A (dark grey), B (grey), and C (light grey), plus the irregular episodes IE (white).

low intensity SED episodes it is not so easy to say whether the SED activity stops when no more SEDs are recorded, whether the strength of the storm has decreased slightly, or whether an ionospheric damping effect on the dayside leads to the suppression of SED intensity below the galactic background noise. Storm D from June 2005 is particularly interesting in this respect, as there are signal intensities up to 14 dB, but the SEDs are gone at the next Saturn rotation. Storm D consists of two very long and two very short episodes: D1 lasted more than 9 h, D3 nearly 7 h, and both D2 and D4 around 3 h. It is possible that D1 had an extended longitude or that it consisted of several smaller longitudinally separated storm cells which, in fact, showed no SED activity at the next Saturn rotation and returned as the short D2 episode about 4.7 Saturn rotations (local time change of spacecraft is included in this calculation) later. As RPWS would have registered very weak SEDs between D1 and D2, it is likely that there was practically no SED activity between D1 and D2. We conclude that there can be significant time variability in the SED storm strength within a time scale of several hours. The D3 episode appeared about 4.0 Saturn rotations after D2 and showed similar intensity, burst rate and episode duration as D1. So the storms can get weaker with no SED activity for several Saturn rotations, but SED activity can reappear again with decreased or increased strength compared to the previous episode. Nevertheless, the short time durations of the episodes in 2004 might only be partly explainable by the intrinsic SED on–off behavior of the storm. Interestingly the mean episode duration of 2 h 53 min is only slightly longer than a quarter of a Saturn rotation. As Cassini is a practically stationary observer at the morning side of Saturn around 06 LT, the mean episode duration is close to the time an SED related storm passes the nightside from Cassini's point of view. We will report later, that a comparison of the visual observation of storm systems in Saturn's atmosphere and the SED occurrence has shown that most SEDs occur during the period when the visible storm system is on the nightside of the planet. Hence,

there should be ionospheric damping and radio wave blockage on the dayside.

5. Physical properties related to the temporal occurrence of SEDs

5.1. Duration of bursts

The receiver sweeps through the frequencies step by step, so an SED burst can cover several successive frequency channels (pixels), although most of the SEDs (about 65%) of 2004 were observed in only one channel ("one pixel bursts"). As four different integration times (10, 20, 40, or 80 ms) can be used, a detection in a single channel can correspond to four different time durations. Only 7 SEDs were registered with the 10-ms integration time, whereas ∼140, ∼4200, and ∼1100 were recorded with the integration times 20, 40, and 80 ms, respectively. A settling time of 5 ms has to be added to the integration time, and so the time duration of the SEDs ranged from 15 to 450 ms. The burst with the longest duration occurred on DOY 257 around 18:50 SCET with an integration time of 40 ms in the frequency range from 12,125 to 13,025 kHz, and it consisted of 10 pixels with a mean intensity of 4 dB above background.

The burst duration is well described by an exponential decrease of the number of events n with increasing time t by $n \propto \exp(-t/t_0)$ with the so-called e-folding time t_0. For the ∼4200 SEDs with an integration time of 40 ms this e-folding time was calculated by a fit to be $t_0^{40\ \mathrm{ms}} = (47 \pm 4)$ ms. For the integration times of 20 ms and 80 ms we obtained $t_0^{20\ \mathrm{ms}} = 40$ ms and $t_0^{80\ \mathrm{ms}} = 48$ ms, respectively, although these two numbers have high errors due to the limited number of bursts in the case of 20 ms and the limited number of channels (maximum only 3) for an integration time of 80 ms. A histogram of the number of bursts as a function of the burst duration can be found in Zarka et al. (2006). They calculated the same e-folding time as in this work for the SEDs of storm C, where the 40-ms integration time was used. We also note that these results are close to the e-folding times of 41 ms for SEDs detected by Voyager 1 and 38 ms for SEDs detected by Voyager 2 as calculated by Zarka and Pedersen (1983). As high time resolution measurements by the Voyagers have shown (Evans et al., 1983), it is likely that each SED is made up of many individual subevents (analogous to multiple strokes in a terrestrial flash).

5.2. Total numbers and SED burst rates

Altogether 5403 SEDs were recorded by Cassini/RPWS in 2004: for storm 0 we found 111 SEDs (∼2%), storm A had 781 SEDs (∼15%), storm B had 269 SEDs (∼5%), storm C had 4167 SEDs (∼77%), and the rest of 75 SEDs (∼1%) belongs to the isolated or irregular SEDs and episodes. Depending on the instrument mode the HFR resides only for a limited time at the frequency range where SEDs can be expected, hence the "true" or "interpolated" SED burst rate should be higher than the "apparent" burst rate, the latter simply calculated by dividing the number of SEDs per episode by the episode duration. At the end of Section 2 we estimated the duty cycle of the various instrument modes for frequencies above 1.8 MHz, and we found 9% for an integration time of 20 ms (storm 0), 36% for an integration time of 40 ms (storm C), and 27% for an integration time of 80 ms (storms A and B). The 4167 SEDs of storm C were recorded during 49 episodes with a total time duration of 175.9 h. But, due to the duty cycle of 36%, the 175.9 h correspond to an actual observing time of only 63.3 h giving a true mean SED burst rate of about 66 h^{-1}. Similarly we find true mean SED burst rates of 87 h^{-1} for storm 0, 78 h^{-1} for storm A, and 30 h^{-1} for storm B, respectively. For all four storms we arrive at a true mean SED burst rate of 64 h^{-1}. The true burst rates for each individual episode can be found in the 7th column of Tables 1 and 2, and it can be seen that true burst rates range from 6 up to 322 h^{-1}, the latter being obtained for episode A1. All episodes with more than 200 SEDs have a burst rate higher than 100 h^{-1}, so episodes with a high number of bursts have also higher burst rates.

6. SED intensity and intensity spectrum

The intensity of the signals from the SEDs in the frequency range from 1 to 16 MHz varied over 2 magnitudes from about 10^{-15} to 10^{-13} $\mathrm{V^2\,Hz^{-1}}$ (Fischer et al., 2006). This is not due to the variation of the SED signal strength, but due to the large gain at the antenna resonances at 9.5 MHz for the monopole and at 8.8 MHz for the dipole (Zarka et al., 2004), which amplifies the SED signals as well as the background near these frequencies. We summarize the results from Section 4 by listing the mean relative intensities in dB above the background of the SEDs of the various storm systems: 1.8 dB for the storm 0 SEDs, 2.4 dB for storm A, 2.2 dB for storm B, 1.6 dB for storm C, 2.5 dB for the irregular or isolated SEDs, and 1.8 dB for all SEDs from 2004. We note that the bursts at the beginning and the end of episodes are generally less intense than in the middle. The peak burst intensities in the middle of the episode can be a factor of 5 above the average intensities at both episode edges. Zarka et al. (2006) explain this by ionospheric propagation effects.

The incident flux and the source powers of the SED signals were evaluated by Zarka et al. (2006) and Fischer et al. (2006) in two independent ways: Zarka et al. (2006) relied on the careful estimation of the receiver background and on the measurement of the galactic background by the RPWS instrument. They related it to the model of the galactic background by Dulk et al. (2001), and in this way the calibrated flux density S in $\mathrm{W\,m^{-2}\,Hz^{-1}}$ of each detected burst can be obtained. They found an average source power of $P \sim 100\ \mathrm{W\,Hz^{-1}}$ for all SEDs of storm C. The source power P is calculated from the flux density S under the assumption of an isotropic emission with the formula $P = 4\pi r^2 S$ with r as the distance between the spacecraft and the surface of Saturn. Fischer et al. (2006) used a wire grid model of the Cassini spacecraft to calculate a reception area of the respective RPWS antenna depending on the direction of wave incidence and on frequency. The calibrated flux density S of the SEDs is obtained by dividing the background subtracted SED signal intensity by the reception area and the impedance of

free space. In this way they found an average source power of 220 W Hz^{-1} for storm 0, 65 W Hz^{-1} for storm A, 145 W Hz^{-1} for storm B, and 40 W Hz^{-1} for storm C, giving an average of 50 W Hz^{-1} for all SEDs of 2004. The difference between the Zarka et al. (2006) and Fischer et al. (2006) result for storm C is partly due to the fact that Zarka subtracted the 5% occurrence level background from the signal, whereas Fischer used the 50% occurrence level background. Nevertheless, considering the general difficulty of absolute flux measurements and the inherent inaccuracies of the antenna modeling and the galactic background model, the agreement of the results between the two completely different approaches is quite good. The average source powers found for the SEDs with Cassini/RPWS are of the same order as the source powers of 100 and 10 W Hz^{-1} for Voyager 1 and 2, respectively (Zarka and Pedersen, 1983).

We note that the supposed SED episode recorded by Cassini/RPWS on July 22, 2003, from a distance of about 1.08 AU (Gurnett et al., 2005) is most likely a jovian emission. The source power of these supposed SEDs would have been monstrous, approximately 10^3 times greater than the source power of all other SEDs. A detailed analysis of this 2003 event will be presented somewhere else and is not subject of this paper.

SEDs are about 10^4 more powerful than terrestrial lightning flashes, when we take the intensity of the radio emissions in the frequency range of a few MHz for comparison. This estimation is based on the different detection distances of terrestrial flashes and SEDs with Cassini/RPWS: During the Earth flyby of Cassini/Huygens in August 1999 signals from terrestrial flashes were recorded up to a distance $d_E \approx 14\ R_E$ (Earth radii) (Gurnett et al., 2001), whereas the first detection of SEDs was at a distance $d_S \approx 378\ R_S$ (Saturn radii) when we regard the 2003 episode as non-SED. As the flux should decrease with distance squared, we calculate the squared ratio of the detection distances: $d_S^2/d_E^2 = (378 \times 60300)^2/(14 \times 6378)^2 \approx 6.5 \times 10^4$. Assuming that the radio flux density in this limited frequency range is proportional to the total energy of the flash, with the same proportional factors for a typical SED as well as for a terrestrial flash, one can estimate the total energy of an SED to be around 10^{13} J. This is a factor of 10^4 above the total energy of 10^9 J of a typical terrestrial flash.

A terrestrial flash has a power spectrum with a spectral energy density peak around 10 kHz (corresponding to a typical discharge time of 100 μs), a decrease with f^{-2} up to about 5 MHz, and a spectral "knee" with a decrease of f^{-4} to f^{-5} at higher frequencies (Willett et al., 1990). We do not know the power spectrum of SEDs at lower frequencies, and in the MHz range the power spectrum of SEDs is different compared to terrestrial flashes: Zarka and Pedersen (1983) calculated a true spectrum for the SEDs, where it turned out that the spectral power is practically constant with frequency f from 5 to 26 MHz. Such a flat spectrum suggests that the initiating discharge must be very fast (Farrell et al., 1999). For example a peak frequency of about 1 MHz corresponds to a typical discharge time of 1 μs, and such a fast discharges could also be powered by flashes with much less total energy than 10^{13} J, assuming that the peak radiated energy is a few percent of the total flash energy. Fischer et al. (2006) found a slight decrease

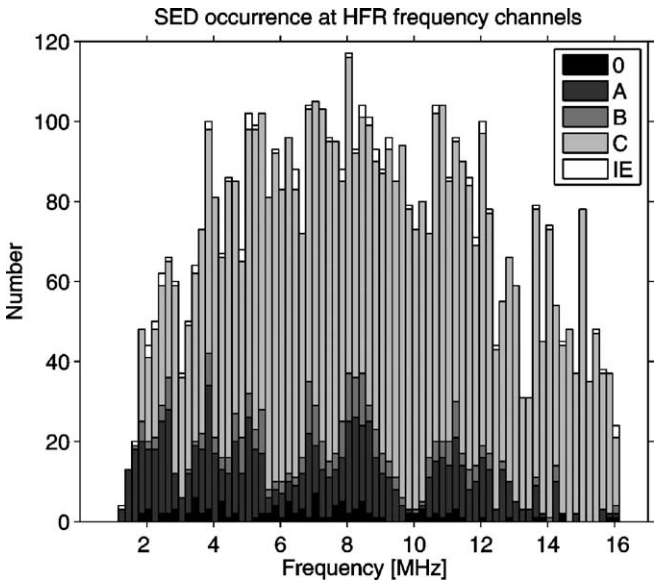

Fig. 8. Stacked bar-plot showing the SED occurrence of all SEDs from 2004 as a function of frequency in bins of 200 kHz. Different storms are characterized by different grey-scale shading as in the previous figure.

with $f^{-0.5}$ in the frequency range of 4–16 MHz for the SEDs from 2004, which is the first hint that the RPWS might sample the "rolloff" side of the spectrum.

Fig. 8 shows the number of SEDs recorded at the various HFR frequency channels from 1.2 to 16.2 MHz in 200 kHz bins in different shading corresponding to the respective storm system. In general one would expect an equal distribution of the SEDs at all frequency channels above the ionospheric cutoff frequency, which is obviously not the case in Fig. 8: At frequencies below 4 MHz the number of SEDs is decreased, which is likely an ionospheric cutoff effect. The second obvious feature of Fig. 8 is the gradual decrease of SED numbers at higher frequencies above 8 MHz. This can be well explained by the rolloff with $f^{-0.5}$ found by Fischer et al. (2006), as $f^{-0.5}$ corresponds to an intensity decrease of 1.5 dB from 8 to 16 MHz, which is enough for many SEDs (mean intensity of 1.8 dB) to drop below the galactic background level.

7. Localization of the SED sources

7.1. Results from imaging observations

From optical observations with the Cassini/ISS (Imaging Science Subsystem) Porco et al. (2005) report a particular active narrow southern mid-latitude region where bright storm eruptions are correlated with Saturn's electrostatic discharges. A storm at 35° South produced eruptions of white material in mid-July corresponding to SED storm A, and again in mid-September, which is clearly correlated to storm C. This storm reached its peak intensity in visible light on days 255–260, and after fading for a few days it returned as high-contrast bright spot on day 269. Especially on DOY 256 and DOY 270 there was an unusual brightening of the storm correlated with peaks in SED occurrence: Fig. 4 or Table 2 show that on DOY 256 episode C19 has more than 300 bursts. Episode C44 on DOY

269 has more than 400 bursts and is surrounded by episodes C43 (DOY 269) and C45 (DOY 270), both with more than 300 SED bursts. SED activity recorded by RPWS stopped on DOY 272, and ISS observed the appearance of a dark filament turning the bright clouds into a dark spot between DOY 272 and 274 (Porco et al., 2005).

An interesting aspect is that the SED episodes generally began about 0.4 planetary rotations before the atmospheric features crossed the central meridian (center of the planetary disc as viewed from Cassini), which means that the SED episodes started in fact before the cloud feature appeared over the nightside horizon. The peak intensity occurred about 0.2 planetary rotations (∼72°) before the central meridian crossing, which could suggest that the SED source is ∼72° to the east of the visible cloud. Porco et al. (2005) suggest that this could be due to a lightning source much deeper than the visible cloud, which trails off to the west because of wind shear. Another possible explanation is that the SED source is approximately at the position of the visible cloud system (possibly 300 km below it), and an ionospheric bending of the rays could extend the radio horizon beyond the visible (geometric) horizon. The SED episodes generally ended about 0.1 planetary rotations after the central meridian crossing of the cloud feature, which in fact means that the cloud was still within the visible horizon of the spacecraft, but there were no SEDs recorded by RPWS anymore. If the SED source was really 0.2 planetary rotations eastward of the visible cloud feature, this would be understandable as the SED source would have already rotated beyond the eastern dayside horizon. But, also in this case there is an alternative explanation suggesting that ionospheric conditions on the dayside lead to the damping of the radio waves.

7.2. SED drivers

Desch et al. (2006) presume that lightning is associated with vertical convection driving moisture up to the visible atmospheric cloud level from the water cloud level, which is at about the 10-bar level approximately 300 km below the 1-bar level. A three-dimensional model of moist convection for Saturn was constructed by Hueso and Sánchez-Lavega (2004) suggesting that very energetic water storms can reach the 150-mbar level, thereby developing vertical peak velocities of the order of 150 $m\,s^{-1}$. Desch et al. (2006) point out that external sunlight is extinguished at pressures greater than 2 bar, and that the UV fluctuations (determined from the 10.7-cm radio flux and CaII–K line proxies for UV flux) that are apparent during 2004 do not match the fluctuations observed in the SED rate, and there might be also no other possible external drivers of the SED activity. The possible depth of 300 km for the SED source implies also the extinction of the optical energy of the SEDs, so we will possibly never succeed in detecting visible wavelength light from Saturn lightning with optical instruments unlike the situation with jovian lightning.

The origin of SEDs from such high pressure levels could also explain why the SEDs are so powerful and in fact relatively rare (when we look at the SED burst rate related to the area of the storm): A higher pressure requires a higher breakdown electric field, and sufficient charge separation to reach this higher field might be a rare event. But when it happens, the discharge is much stronger since the total energy of a discharge is proportional to the neutralized charge, as can be shown by electrostatic model calculations (Cooray, 1997).

Desch et al. (2006) suspect that the most likely internal source of SED energy is the factor 2–3 thermal excess emitted by Saturn which powers the SEDs as well as Saturn's weather in general. On the other hand, the permanent temperature gradient from the sharp ring shadow in the equatorial zone might have been an external trigger of the strong equatorial storm system which is generally thought to be the source of the SEDs in the Voyager era. In the first years of Cassini's tour at Saturn the shadow of the ring system is much broader and located in the northern hemisphere as it is southern summer. At the end of the nominal mission in 2008 the situation will become more Voyager-like, and the equinox with the edge-on ring position will be reached in September 2009. Therefore, we can possibly expect more Voyager-like SED activity towards the end of the Cassini mission.

7.3. The phase shift between the visible cloud feature and the SED occurrence—ionospheric implications

The relative phase of about 0.2 planetary rotations between the visible cloud feature and the SED occurrence is puzzling: A trailing off by 72° corresponds, in fact, to a distance of about 75,000 km along a depth of just 300 km. In their modeling of up-welling water clouds, Hueso and Sánchez-Lavega (2004) include only moderate horizontal velocities and they suggest vertical peak velocities up to 150 $m\,s^{-1}$ (540 $km\,h^{-1}$). A water cloud should need 2–5 h for the up-welling from a depth of about 300 km (see Table 2 of Hueso and Sánchez-Lavega, 2004), as the average velocity is less than the peak velocity. Also the imaging observations have shown that this modeling is quite reasonable, as there seems to be no time shift (probably just a few hours) between the peak occurrence of SEDs on the days 256 and 270 and the unusual brightening of the visible cloud features. So how can an SED source at a distance of 75,000 km influence a visible cloud feature within such a short time? We suggest that it cannot, because this would require unrealistically high westward wind speeds at deeper levels at this latitude, where a zero zonal wind speed has been measured for the surface features. As already mentioned, a longitudinal extension of about 72° of the SED source is unlikely due to the relatively short episode durations displayed in Fig. 7 with a mean value of just 3.6 h for storm C. Also, the images show no indication of a longitudinally extended storm. We conclude that both scenarios, an SED source shifted by 72° to the east as well as a longitudinally extended SED source, are unlikely.

For the electrification of particles in thunderstorms there are the so-called precipitation theories in lightning physics, where falling precipitation particles interact with lighter particles carried in updrafts (Rakov and Uman, 2003). Therefore it is likely that SEDs are directly connected with the updraft of water clouds as they were modeled by Hueso and Sánchez-Lavega (2004) and observed by Porco et al. (2005). Perhaps some in-

formation about the time scale of such updrafts can be gained by a careful comparison of the SED occurrence and the brightness of the cloud feature as a function of time.

As already mentioned, the puzzling phase shift could be well explained by ionospheric propagation effects: Zarka et al. (2006) point out that there could be a decrease of ionospheric electron density with increasing local time right after midnight towards the early morning side. This could cause an escape of radio waves after being temporarily trapped, and would explain the start of SED episodes with the SED source still below the visible horizon. At the disappearance of SEDs on the dayside there is not only ionospheric damping but also the angle between the ray and the normal to the ionosphere is increasing leading to a higher cutoff frequency. Seen from the local time position of Cassini on the morning side, the SED source was rotating from the nightside to the dayside of the planet under an ionosphere with gradually increasing electron density on the dayside. This results in a gradually increasing low-frequency cutoff with time as can be seen quite well for episode C43 in Fig. 6 but also for episode 07 in Fig. 1. Not every episode behaves like this, but the rising low-frequency cutoff with time is evident for most of the episodes with a duration longer than 4 h.

7.4. Polarization and DF measurements of SEDs

During the SED storms A and B in 2004 the HFR of the RPWS instrument was in the so-called direction-finding (DF) mode, where a determination of the direction of incidence and the polarization of the radio waves is possible. Nevertheless the DF-technique has also certain limits: Firstly for storms A and B the spacecraft was further out than 80 Saturn radii, and from this distance the disc of Saturn appears at an angle smaller than 1.5°, which approximately equals the error of the DF-technique. So it would be only possible to show that the radio waves stem from Saturn, and no further conclusions about latitude and longitude of the storm can be drawn. Meaningful DF results for tracking an SED storm can only be obtained inside of about 10 Saturn radii. Secondly, the DF technique works only for frequencies less than 2 MHz since for greater frequencies the wavelengths approach the dimension of the antennas and the spacecraft, leading to a complex antenna beam pattern. Thirdly, the signal intensities should be 10–15 dB above the background to get reasonable errors for direction-finding and polarization measurement (Cecconi and Zarka, 2005), which also requires a spacecraft closer to Saturn. In 2004 only 85 SED bursts below 2 MHz with a mean intensity of 2.2 dB above background have been measured by RPWS. Finally, we note that although the direction-finding capability of the RPWS has not led to a proof for the atmospheric storm explanation until now, the direct correlation of a visible cloud feature with the SED occurrence as well as the behavior of the low-frequency cutoff of SED signals completely rule out the exotic SED ring source hypothesis.

8. Periodicity of the SED episodes

The permanent presence of the SEDs and the sufficient number of highly regular episodes during the Voyager 1 encounter had the advantage that it was possible to derive the rotation period of 10 h and 10 min of the SED storm system with reasonable accuracy. This became more difficult for the Voyager 2 encounter as the episodes did not show the typical on–off behavior anymore. From a periodicity analysis Zarka and Pedersen (1983) derived an episode recurrence period for Voyager 2 of 10 h with an error of about ±7 min. This number has to be taken with care, because a recurrence period of exactly 10 h would imply wind speeds up to 650 $m\,s^{-1}$, and such high wind speeds (about 2300 $km\,h^{-1}$) have never been measured in Saturn's atmosphere. For Cassini, a determination of the episode periodicity must be done with care since the SED episodes were not permanently present, and in some cases there are only few episodes. Additionally, with the mean episode duration of less than 3 h, we do not know exactly at which local time and longitudes of Saturn the storm system is located during the SED activity. Nevertheless, a typical feature of some episodes is an abrupt onset, which is consistent with a source that has just risen over the radio horizon (Desch et al., 2006). So for these episodes we can infer the western longitude of the source at a given instant of time.

Fig. 9 shows the sub-spacecraft western longitude (not to mix up with the western longitude of the storm itself) of Cassini as a function of time given in Saturn rotations during the various episodes of storms 0, A, B, and C. The stars denote the sub-spacecraft western longitude at the center times of the episodes, and a certain fluctuation of the phase is evident. The lines (dotted, dashed, or solid corresponding to the number of SEDs per episode) give the longitude range from the first to the last SED of the episode. As shown in Fig. 9 the sub-spacecraft western longitudes at the onsets of the storm C episodes are relatively constant (around 190°). In these plots it is possible to make a linear fit of the episode centers or edges with time and to calculate a recurrence period from the slope of the fitted straight line. Using the episode centers one arrives at periods of (10.59 ± 0.09) h for storm 0, (10.71 ± 0.03) h for storm A, (10.66 ± 0.03) h for storm B, and (10.66 ± 0.01) h for the prominent storm C (excluding the irregular episodes during the various storms). Making a fit of all 88 episodes excluding only the 7 irregular ones, the result is (10.660 ± 0.002) h, which is practically the Voyager radio period. There are some zonal belts at various latitudes (around 35°, 50°, 65°, and 75° North and South) of Saturn, where the atmospheric winds match the Voyager radio period. We note that there would be a substantial drift of western longitude with time in Fig. 9 when using a western longitude counting based on the slower Cassini SKR radio period. Nevertheless, the periodicity analysis would give the same results for the various SED storms as listed above.

In general, a shift of the sub-spacecraft western longitude of the episode center or edges from one Saturn rotation to the next can have different reasons related to the SED source itself or to propagation effects:

(1) The internal triggering mechanism can be variable in time at a time scale of hours leading to an onset and disappearance of the SED episodes at arbitrary local times of Saturn,

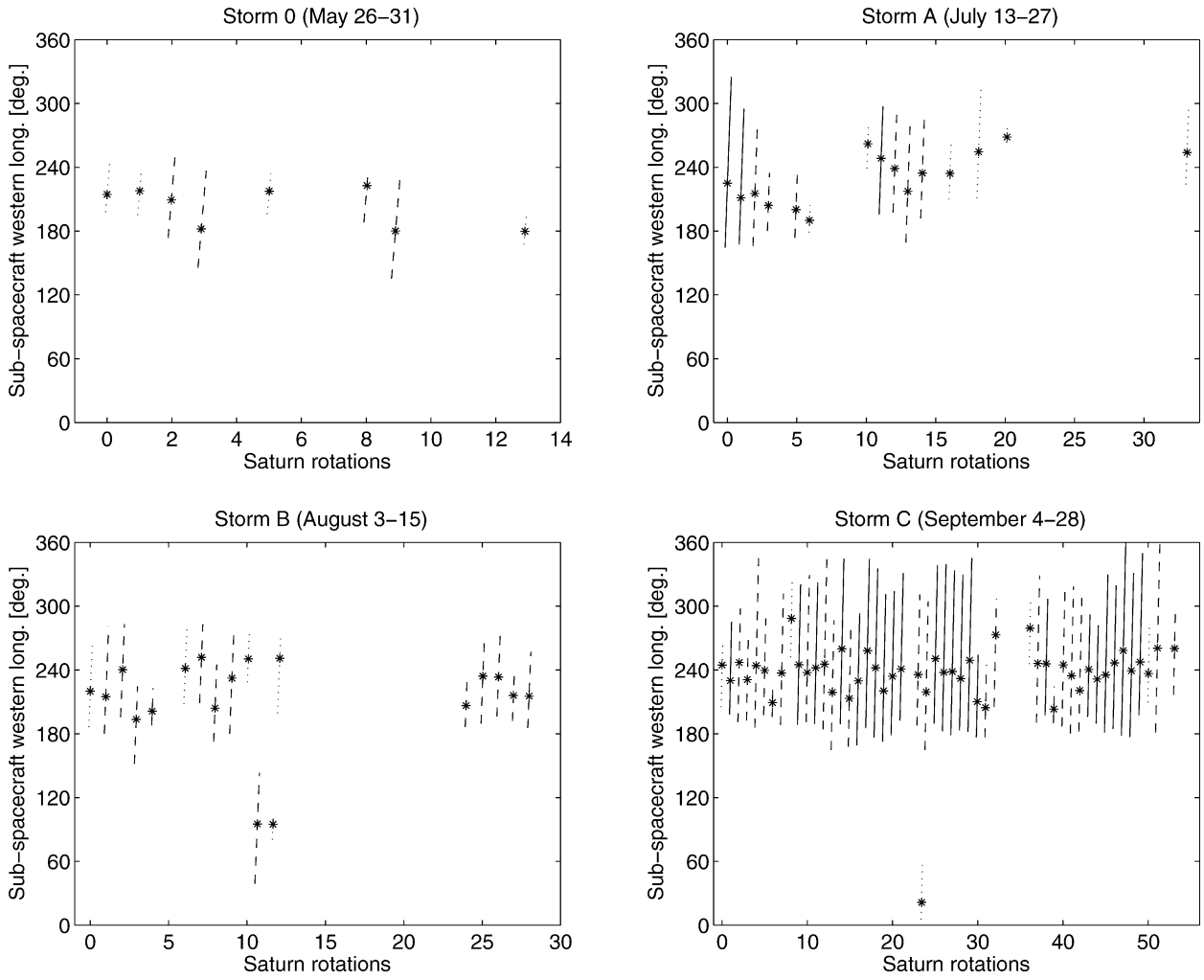

Fig. 9. Sub-spacecraft western longitude ranges for the various episodes of the 4 storms 0, A, B, and C in 2004 as a function of time displayed in units of Saturn rotations. The star denotes the so-called center time, which is the mean time of all SED bursts within one episode. The time in Saturn rotations is set to 0 at the center time of the first episode of each storm. The lines indicate the sub-spacecraft western longitude range from the first to the last SED of the respective episode. Dotted lines denote weak episodes with less than 10 bursts, dashed lines denote intermediate episodes with greater than or equal to 10 but less than 50 bursts, and solid lines denote episodes with 50 and more SED bursts.

(2) changing ionospheric conditions at successive Saturn rotations leading to radio horizons at different local times of Saturn,
(3) variation of the SED source strength with time which shifts the episode centers,
(4) several smaller stormy areas at different longitudes with SED activity at different times, and of course also
(5) a rotation period of the SED source different from Saturn of storms located in a non-zero wind band.

Good accuracy in the periodicity analysis can be obtained with a sufficiently large number of episodes occurring at nearly every Saturn rotation, which is the case for storm C. The constant sub-spacecraft western longitude with time for storm C indicates a rotation with Saturn's Voyager radio period, hence, the storm should be located at a latitude with a zonal wind velocity close to zero, which is consistent with the visual observations of clouds at 35° South. For storm 0 there are only 8 episodes with a mean duration of just 1.8 h, and the variation of the episode center with time might be caused by one or several points in the above list. Storm A seems to consist of 2 parts, plus the last episode A15, and the second part A7 to A14 is slightly shifted towards greater longitudes with regard to the first part A1 to A6. The constant decrease of sub-spacecraft western longitude for A1 to A6 and later also for A7 to A10, which is followed by an increase from A10 to A14, is rather puzzling. It might be caused by points (1)–(4) but possibly not by point (5) from the list above, as the overall behavior of storm A is a rotation with the Voyager radio period consistent with the visual observations of clouds at 35° South. Storm B seems to consist of 3 parts (B1 to B5, B6 to B11, and B12 to B16) and there is no clear drift within one of these three parts but rather some kind of oscillation. There are two irregular episodes IE5 and IE6 within storm B possibly caused by a second small storm system at a different western longitude.

It can be seen even more clearly in Fig. 10 that all four storm systems are in a similar sub-spacecraft western longitude range. This figure is a stacked histogram plot showing the number of

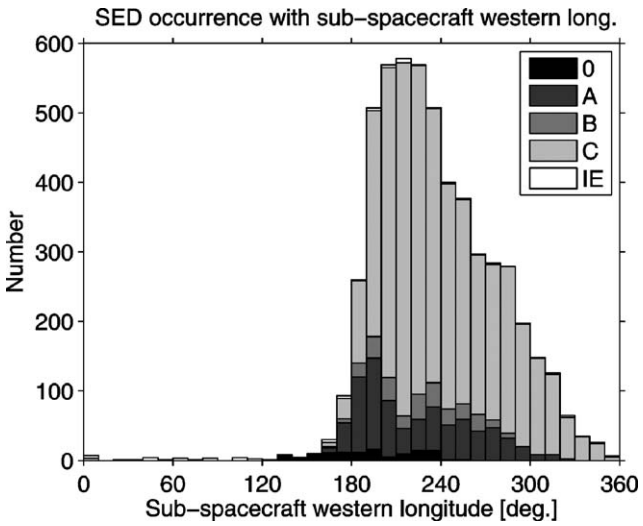

Fig. 10. Stacked bar-plot showing SED occurrence of all SEDs from 2004 with sub-spacecraft western longitude in bins of 10°. Different storms are characterized by different grey-scale shading as in previous figures.

SEDs as a function of the sub-spacecraft western longitude in 10° bins, and the storms can be identified through the different grey-shading. The irregular SEDs not belonging to one of the storm systems are distributed over all longitude ranges. The prominent storm C has some episodes with a duration longer than 4 h, hence, its western longitude range is slightly more extended than those of the other storms. The SEDs of storm 0 occur at a mean sub-spacecraft western longitude of $194° \pm 30°$, of storm A at $224° \pm 37°$, of storm B at $226° \pm 29°$, and of storm C at $242° \pm 38°$, with the error as the 1σ standard deviation. Taking all SEDs except the irregular ones, the mean longitude is $238° \pm 39°$. There is a gradual increase in mean sub-spacecraft western longitude from storm 0 to storm C of more than 40°. The calculated period of 10.660 h of all 4 storms is slightly longer than the Voyager radio period of 10.656 h leading to this 40° increase in western longitude in a time interval of 125 days from the start of storm 0 on DOY 147 to the end of storm C on DOY 272.

9. A hypothesis on the location of the SED storms of 2004

Assuming that the four SED storms have developed from independent cloud systems at different regions, it would be a rather improbable coincidence that they were all recorded in the same sub-spacecraft western longitude range. There were practically no SEDs in the longitude range from 0° to 150° in 2004 as can be seen in Fig. 10. Storm D from June 2005 (not shown in Fig. 10), resides mainly at a different sub-spacecraft longitude range from about 0° to 200°, although this range might be shifted by nearly ±40° due to the gap of more than 570 Saturn rotations between storms C and D and the uncertainty of the Voyager radio period (on which the counting of the longitude system is based) by ±7 s (Desch and Kaiser, 1981). We already mentioned that storms A and B are somehow connected by episode A15, which appears in phase 13.0 Saturn rotations after A14 and 13.9 Saturn rotations before B1. Since we have a visual suggestion for storms A and C residing at a latitude of 35° South, and storm B in-between is at the same longitude range with virtually no drift with time, we give the following hypothesis: The SED storms A, B, and C originate from the same atmospheric storm system residing at a latitude of 35° South. Storm 0 possibly also belongs to it, although there is a slight shift in sub-spacecraft western longitude and there are approximately 6 weeks between the end of SED storm 0 and the start of SED storm A. The overall atmospheric storm system lasted for several months, it waxed and waned in strength with different levels of SED activity, and it rotated with the Voyager radio period of Saturn. Perhaps visual confirmation could be also found for the SED storms 0 and B, which would confirm or reject this hypothesis.

10. Conclusion and outlook

This paper is a straightforward tabulation and organization of the data returned from Cassini's RPWS instrument in 2004 concerning the SEDs (Saturn Electrostatic Discharges), which are associated with lightning flashes in Saturn's atmosphere. About 5400 SEDs were extracted from the RPWS data by applying a computer algorithm with intensity thresholds depending on the receiver integration time. One of the most striking features was the time variability of the SEDs: They appeared in 4 storm systems consisting of 95 episodes in total, and there were significant time intervals with no SED activity, e.g., SEDs were practically absent from October 2004 until June 2005. Also the burst rates of the episodes showed a high variability, ranging from a few bursts per hour to more than 300 SEDs per hour. Further characteristics of the episodes have been listed in detail in Tables 1 and 2. SED characteristics like the burst duration (e-folding time of (47 ± 4) ms for SEDs of the September storm), and the absolute intensity (50 $\mathrm{W\,Hz^{-1}}$) were similar to the SEDs observed by both Voyagers. The Cassini SEDs appeared just a few dB above the galactic background due to the greater distance of at least 75 Saturn radii of Cassini to Saturn during the SED detections. Another striking difference to the Voyagers was the mean duration of SED episodes, which was below 3 h indicating a rather localized SED source and a crucial influence of Saturn's ionosphere. We emphasized that all SEDs from 2004 most likely stem from a single atmospheric storm system residing at a latitude of 35° South. This storm system lasted for several months, waxed and waned in strength, and rotated with the Voyager radio period of Saturn. We favor the explanation that the SEDs are the radio signature of lightning flashes from storms in Saturn's atmosphere. The source might be located at up-welling water clouds beneath the visible cloud features detected in the Cassini images. Detailed correlation studies between the occurrence of SEDs and visible cloud features in the images should be carried out in future. Additionally, the capability of the RPWS to measure the polarization of the SEDs and the determination of the direction of incidence of the radio waves can be used in future if SEDs appear at a sufficient intensity level when Cassini is closer to Saturn. Attempts are under way to detect SEDs also with Earth-based ground telescopes in the decametric frequency range.

References

Burns, J.A., Showalter, M.R., Cuzzi, J.N., Durisen, R.H., 1983. Saturn's electrostatic discharges: Could lightning be the cause? Icarus 54, 280–295.

Cecconi, B., Zarka, P., 2005. Direction finding and antenna calibration through analytical inversion of radio measurements performed using a system of 2 or 3 electric dipole wire antennas. Radio Sci. 40 (3), doi:10.1029/2004RS003070. RS3003.

Cook, A.F., Duxbury, T.C., Hunt, G.E., 1979. First results on jovian lightning. Nature 280, 794–795.

Cooray, V., 1997. Energy dissipation in lightning flashes. J. Geophys. Res. 102 (D17), 21401–21410.

Desch, M.D., Kaiser, M.L., 1981. Voyager measurement of the rotation period of Saturn's magnetic field. Geophys. Res. Lett. 8 (3), 253–256.

Desch, M.D., Fischer, G., Kaiser, M.L., Farrell, W.M., Kurth, W.S., Gurnett, D.A., Zarka, P., Lecacheux, A., Porco, C., Ingersoll, A., Dyudina, U., 2006. Cassini RPWS and imaging observations of Saturn lightning. In: Rucker, H.O., Kurth, W.S., Mann, G. (Eds.), Planetary Radio Emissions VI. Austrian Academy of Sciences Press, Vienna. In press.

Desch, S.J., Borucki, W.J., Russell, C.T., Bar-Nun, A., 2002. Progress in planetary lightning. Rep. Prog. Phys. 65, 955–997.

Dulk, G.A., Erickson, W.C., Manning, R., Bougeret, J.-L., 2001. Calibration of low-frequency radio telescopes using the galactic background radiation. Astron. Astrophys. 365, 294–300.

Evans, D.R., Warwick, J.W., Pearce, J.B., Carr, T.D., Schauble, J.J., 1981. Impulsive radio discharges near Saturn. Nature 292, 716–718.

Evans, D.R., Romig, J.H., Hord, C.W., Simmons, K.E., Warwick, J.W., Lane, A.L., 1982. The source of Saturn electrostatic discharges. Nature 299, 236–237.

Evans, D.R., Romig, J.H., Warwick, J.W., 1983. Saturn's electrostatic discharges: Properties and theoretical considerations. Icarus 54, 267–279.

Farrell, W.M., Kaiser, M.L., Desch, M.D., 1999. A model of the lightning discharge at Jupiter. Geophys. Res. Lett. 26 (16), 2601–2604.

Fischer, G., Macher, W., Desch, M.D., Kaiser, M.L., Zarka, P., Kurth, W.S., Farrell, W.M., Lecacheux, A., Cecconi, B., Gurnett, D.A., 2006. On the intensity of Saturn lightning. In: Rucker, H.O., Kurth, W.S., Mann, G. (Eds.), Planetary Radio Emissions VI. Austrian Academy of Sciences Press, Vienna. In press.

Gurnett, D.A., Shaw, R.R., Anderson, R.R., Kurth, W.S., 1979. Whistlers observed by Voyager 1—Detection of lightning on Jupiter. Geophys. Res. Lett. 6, 511–514.

Gurnett, D.A., Zarka, P., Manning, R., Kurth, W.S., Hospodarsky, G.B., Averkamp, T.F., Kaiser, M.L., Farrell, W.M., 2001. Non-detection at Venus of high-frequency radio signals characteristic of terrestrial lightning. Nature 409, 313–315.

Gurnett, D.A., Kurth, W.S., Kirchner, D.L., Hospodarsky, G.B., Averkamp, T.F., Zarka, P., Lecacheux, A., Manning, R., Roux, A., Canu, P., Cornilleau-Wehrlin, N., Galopeau, P., Meyer, A., Boström, R., Gustafsson, G., Wahlund, J.-E., Aahlen, L., Rucker, H.O., Ladreiter, H.P., Macher, W., Woolliscroft, L.J.C., Alleyne, H., Kaiser, M.L., Desch, M.D., Farrell, W.M., Harvey, C.C., Louarn, P., Kellogg, P.J., Goetz, K., Pedersen, A., 2004. The Cassini radio and plasma wave science investigation. Space Sci. Rev. 114, 395–463.

Gurnett, D.A., Kurth, W.S., Hospodarsky, G.B., Persoon, A.M., Averkamp, T.F., Cecconi, B., Lecacheux, A., Zarka, P., Canu, P., Cornilleau-Wehrlin, N., Galopeau, P., Roux, A., Harvey, C., Louarn, P., Boström, R., Gustafsson, G., Wahlund, J.-E., Desch, M.D., Farrell, W.M., Kaiser, M.L., Goetz, K., Kellogg, P.J., Fischer, G., Ladreiter, H.-P., Rucker, H.O., Alleyne, H., Pedersen, A., 2005. Radio and plasma wave observations at Saturn from Cassini's approach and first orbit. Science 307, 1255–1259.

Hueso, R., Sánchez-Lavega, A., 2004. A three-dimensional model of moist convection for the giant planets. II. Saturn's water and ammonia moist convective storms. Icarus 172, 255–271.

Kaiser, M.L., Connerney, J.E.P., Desch, M.D., 1983. Atmospheric storm explanation of saturnian electrostatic discharges. Nature 303, 50–53.

Mendillo, M., Moore, L., Clarke, J., Mueller-Wodarg, I., Kurth, W.S., Kaiser, M.L., 2005. Effects of ring shadowing on the detection of electrostatic discharges at Saturn. Geophys. Res. Lett. 32, doi:10.1029/2004GL021934. L05107.

Porco, C.C., Baker, E., Barbara, J., Beurle, K., Brahic, A., Burns, J.A., Charnoz, S., Cooper, N., Dawson, D.D., Del Genio, A.D., Denk, T., Dones, L., Dyudina, U., Evans, M.W., Giese, B., Grazier, K., Helfenstein, P., Ingersoll, A.P., Jacobson, R.A., Johnson, T.V., McEwen, A., Murray, C.D., Neukum, G., Owen, W.M., Perry, J., Roatsch, T., Spitale, J., Squyres, S., Thomas, P., Tiscareno, M., Turtle, E., Vasavada, A.R., Ververka, J., Wagner, R., West, R., 2005. Cassini Imaging Science: Initial results on Saturn's atmosphere. Science 307, 1243–1247.

Rakov, V.A., Uman, M.A., 2003. Lightning, Physics and Effects. Cambridge Univ. Press, Cambridge.

Seidelmann, P.K., Abalakin, V.K., Bursa, M., Davies, M.E., de Bergh, C., Lieske, J.H., Oberst, J., Simon, J.L., Standish, E.M., Stooke, P., Thomas, P.C., 2002. Report of the IAU/IAG Working Group on cartographic coordinates and rotational elements of the planets and satellites: 2000. Celest. Mech. Dynam. Astron. 82, 83–110.

Vogl, D.F., Cecconi, B., Macher, W., Zarka, P., Ladreiter, H.-P., Fedou, P., Lecacheux, A., Averkamp, T., Fischer, G., Rucker, H.O., Gurnett, D.A., Kurth, W.S., Hospodarsky, G.B., 2004. In-flight calibration of the Cassini–Radio and Plasma Wave Science (RPWS) antenna system for direction-finding and polarization measurements. J. Geophys. Res. 109, doi:10.1029/2003JA010261. A09S17.

Warwick, J.W., Pearce, J.B., Evans, D.R., Carr, T.D., Schauble, J.J., Alexander, J.K., Kaiser, M.L., Desch, M.D., Pedersen, B.M., Lecacheux, A., Daigne, G., Boischot, A., Barrow, C.W., 1981. Planetary radio astronomy observations from Voyager 1 near Saturn. Science 212, 239–243.

Willett, J.C., Bailey, J.C., Leteinturier, C., Krider, E.P., 1990. Lightning electromagnetic radiation field spectra in the interval from 0.2 to 20 MHz. J. Geophys. Res. 95, 20367–20387.

Zarka, P., 1985a. Directivity of Saturn electrostatic discharges and ionospheric implications. Icarus 61, 508–520.

Zarka, P., 1985b. On detection of radio bursts associated with jovian and saturnian lightning. Astron. Astrophys. 146, L15–L18.

Zarka, P., Pedersen, B.M., 1983. Statistical study of Saturn electrostatic discharges. J. Geophys. Res. 88 (A11), 9007–9018.

Zarka, P., Cecconi, B., Kurth, W.S., 2004. Jupiter's low-frequency radio spectrum from Cassini/Radio and Plasma Wave (RPWS) absolute flux density measurements. J. Geophys. Res. 109, doi:10.1029/2003JA010260. A09S15.

Zarka, P., and the Cassini/RPWS Team, 2006. Physical properties and detection of Saturn's radio lightning. In: Rucker, H.O., Kurth, W.S., Mann, G. (Eds.), Planetary Radio Emissions VI. Austrian Academy of Sciences Press, Vienna. In press.